



This is a repository copy of *Co-assembly and structure of sodium dodecylsulfate and other n-alkyl sulfates in glycerol : n-alkyl sulfate-glycerol crystal phase*.

White Rose Research Online URL for this paper:
<https://eprints.whiterose.ac.uk/172948/>

Version: Accepted Version

Article:

Cosby, J., Starck, P., Littlewood, D. et al. (2 more authors) (2021) Co-assembly and structure of sodium dodecylsulfate and other n-alkyl sulfates in glycerol : n-alkyl sulfate-glycerol crystal phase. *Journal of Colloid and Interface Science*, 596. pp. 442-454. ISSN 1095-7103

<https://doi.org/10.1016/j.jcis.2021.03.063>

© 2021 Elsevier. This is an author produced version of a paper subsequently published in *Journal of Colloid and Interface Science*. Uploaded in accordance with the publisher's self-archiving policy. Article available under the terms of the CC-BY-NC-ND licence (<https://creativecommons.org/licenses/by-nc-nd/4.0/>).

Reuse

This article is distributed under the terms of the Creative Commons Attribution-NonCommercial-NoDerivs (CC BY-NC-ND) licence. This licence only allows you to download this work and share it with others as long as you credit the authors, but you can't change the article in any way or use it commercially. More information and the full terms of the licence here: <https://creativecommons.org/licenses/>

Takedown

If you consider content in White Rose Research Online to be in breach of UK law, please notify us by emailing eprints@whiterose.ac.uk including the URL of the record and the reason for the withdrawal request.



eprints@whiterose.ac.uk
<https://eprints.whiterose.ac.uk/>

Co-assembly and Structure of Sodium Dodecylsulfate and other *n*-Alkyl Sulfates in Glycerol: *n*-Alkyl Sulfate-Glycerol Crystal Phase

James Cosby^a, Pierre Starck^b, Dave Littlewood^b, Oleksandr O. Mykhaylyk^{a*} and Anthony J. Ryan^a

^aDepartment of Chemistry, The University of Sheffield, Sheffield, S3 7HF, U.K.

^bUnilever Research Port Sunlight, Quarry Road East, Bebington, Wirral CH63 3JW, U.K.

*Corresponding author. E-mail: O.Mykhaylyk@sheffield.ac.uk Tel: +44 (0)114 2229418

Abstract

Hypothesis

Following the observation of a microfibrillar phase in sodium dodecylsulfate (SDS)-glycerol mixtures, it is hypothesized that this phase is a crystalline structure containing SDS and glycerol, where the interaction between sulfate and glycerol layers mediates the co-assembly, which also could be universal for similar systems formed by *n*-alkyl sulfate homologues.

Experiment

n-alkyl sulfate glycerol solutions were studied using a combination of optical microscopy, small- and wide-angle X-ray scattering (SAXS/WAXS). Time-resolved SAXS was employed to determine the phase formation in SDS-glycerol-water mixtures.

Findings

The microfibrillar crystalline phase was reproduced in even-chained *n*-alkyl sulfates with a chain length between 12 and 18 carbon atoms, where the phase lamellar period increased uniformly with the alkyl chain length. Reconstruction of electron density profiles from the diffraction patterns allowed the lamellar structural motif of the phase, the glycerol location and stoichiometry to be determined. When SDS-glycerol-water mixtures with water concentration below 6wt% are isothermally solidified at 20°C, SDS-glycerol crystals and/or anhydrous SDS form, where the former is inhibited by the latter at higher water concentrations. The learnings from the SDS-glycerol phase formation allows new gels to be created, utilising the glycerol-sulfate motif generating microfibrils. This expands the knowledge of the applicable formulation space for SDS-water containing mixtures.

Keywords

Glycerol, SDS, Alkyl sulfate, Water, Crystal, SAXS, Microscopy, LMWG, Diffraction, Electron density profile

1. Introduction

Sodium dodecylsulfate (SDS) and glycerol are two ubiquitous materials in the personal care industry with a combined market size of \$3 billion [1–4]. SDS, a surfactant, is commonly used for foaming and detergency, whereas glycerol is a humectant. Both materials are typically used in aqueous or mixed systems with glycerol acting as a minor cosolvent [5,6]. However, anhydrous or polyol rich formulations are now being utilised in applications where water is excluded to gain a therapeutic benefit, such as non-aqueous delivery systems, or personal care formulations [7,8].

The phase behaviour of SDS/glycerol/water mixtures have been well described by numerous authors [9–12]. Khan *et al.* showed that moving from water to glycerol at 1 wt% SDS causes the Krafft temperature to almost double due to the reduced polarity and ionizability of glycerol [13]. This illustrates the challenge in using surfactants designed to work in aqueous systems in an anhydrous milieu, as the stability of mixtures containing SDS in solid form is significantly altered at room temperature [14]. Further work by Matthew *et al.* [15] developed this understanding, showing existence of a 'microfibrillar gel' forming in anhydrous glycerol when solutions of SDS are cooled in glycerol hypothesising that glycerol and SDS combine in a paracrystalline manner, whereby glycerol is found in between crystalline SDS bilayers. However, detailed structural insights into this phase have not been presented. SDS is also known to form well-defined co-crystals with a range of phenolic compounds, as documented by Hirata and Iimura [16]. These morphologies are in stark contrast to the SDS-glycerol microfibrillar phase [15], forming well defined lower aspect ratio

crystals that do not gel. This provides a valuable counterpoint when considering the potential range of structures accessible to SDS.

Similar behaviour to the SDS-glycerol phase can also be observed in the crystallisation of polyols with other charged soaps, such as sodium stearate [17]. Whereby inclusion of solvent (namely water) can lead to high aspect ratio crystals that entangle and gel [18]. Despite some divergence over the degree of crystallinity that these phases represent, an intersecting phenomenon that they can be referred to is coagelation [19–21]. Coagels are typically co-crystalline or co-semicrystalline amphiphiles that have complexed with solvent molecules, to form high aspect ratio aggregates. A typical example is ascorbate based surfactants, which self-assemble with water to form straight 'ribbon' aggregates [22,23]. However, gelation derived from the self-assembly of small molecules could have different formation mechanisms resulting in varying degrees of order and crystallinity [24]. Along with coagels, all small-molecule-based gels are encompassed under the broad terms of molecular gels or low molecular weight gelators (LMWG). Both terms include nanosized hierarchical assemblies where noncovalent interactions allow for supramolecular self-assembly, which consequently controls rheological properties of material at a macroscale. This notably contains self-assembled fibrillar networks [25], wherein one-dimensional nano- or microfibrillar architectures cause gelation [26]. Thus the LMWG effect on structure and rheological properties of materials has meaningful implications for personal care products and formulation science [18,27]. In this respect, the term 'gel' is used in this work to describe the macroscale appearance and properties of a material formed by liquid-arresting self-assemblies of molecules, whereas the term 'crystal' is used to describe a structural organisation with periodic long-range order.

The formation of self-assembled systems can be rationalised through the interactions of its constituents, which must overcome the entropic penalty of organisation and the non-covalent bonding between solvent and solute. In the case of coagels, a high hydrogen bond density is often present, which may be found on either the solvent, in the case of the SDS-glycerol phase, or on the surfactant, in the case of ascorbate-based surfactants and water [28–30].

Further evidence of the importance of multiple hydrogen bonding sites is exemplified by cetyltrimethylammonium bromide (CTAB) and disodium 4, 4'-azobenzene dicarboxylate, whereby nanofiber formation is mediated via CTAB headgroup and carboxy-terminus of the azobenzene [31]. While hydrogen bonding still exists between components within the solution phase, e.g. interactions between solute and bulk solvent, it is conceivably the high density of concurrent interactions facilitated through multiple bonding sites, when geometrically viable, allows for self-assembly to take place. This would further suggest that head-solvent interactions are equally as important as the packing and geometry of hydrophobic tails. Which is in turn evidenced by the wide range of tail geometries that exhibit self-assembly in ascorbate based surfactants [29,30].

The interactions between SDS and water show that the structures formed are clearly path-dependent; the cooling rate and other processing parameters play an important role in defining the polymorph or form of surfactant crystals, with varying degrees of hydration accessible through altered cooling regimes [32,33]. Considering the effect of cooling rate and temperature on the degree of hydration in aqueous systems; it is more than likely that cooling-dependant crystallisation will also occur in mixed aqueous systems. Nevertheless, self-assembly of surfactants can be altered or even hindered by choice of co-solvent, therefore further complicating matters [34].

The structural characterisation of amphiphile crystals and gel phases have been attempted using a variety of techniques. Small- and wide-angle x-ray scattering (SAXS and WAXS) and, in particular, diffraction (SAXD and WAXD), as a result of scattering by a periodic structure, is often used to probe the transition between micellar dispersions and crystalline phases, with neutron scattering techniques also being used [35–37]. If a periodic lamellar-like structure is formed (in either crystalline or liquid crystalline state) by molecules with a long aspect ratio such as hydrocarbons, it is possible to extract information about the molecular packing along the layer normal. This is obtained by reconstructing the electron density (ED) distribution from lamellar diffraction peaks using a Fourier transform [38,39]. Differential scanning calorimetry (DSC) can also be used to study the transition between phases, whereas

microscopy is typically used to identify microscale morphology during (or after) crystallisation [40,41].

In the case of the 'microfibrillar gel' formed from SDS and glycerol, neutron diffraction has been used to determine an SDS bilayer spacing of 48.1 Å and an interlayer glycerol spacing of 7 Å. Building on this knowledge, SAXD and WAXD are used herein to determine molecular packing and geometry to further elucidate the microstructure of SDS-glycerol phase that readily forms a microfibril morphology. Furthermore, we study a homologous series of *n*-alkyl sulfates, exploring the effect of *n*-alkyl chain length on structure, in order to develop a better understanding of the nature of the interactions between *n*-alkyl sulfate surfactants and glycerol. Due to the high purity of SDS compared to other *n*-alkyl surfactant homologues available for this study, and as a result a better quality diffraction data, a detailed structural analysis was focused on the SDS systems. Finally, the effect of water on the SDS-glycerol microfibril formation is quantified using isothermal crystallisation, demonstrating why this phase is not present in mixtures containing very small amounts of water and providing insights into why it has been so elusive.

2. Materials and methods

2.1 Materials

Sodium decylsulfate [$\text{CH}_3(\text{CH}_2)_9\text{OSO}_3\text{Na}$, purity > 99 %], Sodium dodecylsulfate [$\text{CH}_3(\text{CH}_2)_{11}\text{OSO}_3\text{Na}$, > 99 %], Sodium tetradecylsulfate [$\text{CH}_3(\text{CH}_2)_{13}\text{OSO}_3\text{Na}$, > 95 %], sodium hexadecylsulfate [$\text{CH}_3(\text{CH}_2)_{15}\text{OSO}_3\text{Na}$, ~ 60 %], sodium octadecylsulfate [$\text{CH}_3(\text{CH}_2)_{17}\text{OSO}_3\text{Na}$, > 93 %], glycerol (> 99.5 %), water (HPLC grade) were purchased from Sigma Aldrich. The formation of alkyl sulfate-glycerol crystals is strongly dependent on the presence of small amounts of water. To minimise the impact of water, the materials were dried in a vacuum oven at 60 °C for 12 hours before usage. Water content was measured in

glycerol using Karl Fisher titration. Vacuum distillation was used to reduce the water level below 0.5 wt%.

2.2 Preparation of *n*-alkyl sulfate gel phase

The *n*-alkyl sulfate and glycerol were first weighed into glass vials equipped with a magnetic stirrer. Water, where required, was added thereafter. The vessel was then sealed, and the mixture was heated to 60 °C for SDS or 100 °C for all other homologues in an oil bath while stirring for 30 minutes. The vessel with the sample was then removed from the oil bath before cooling to room temperature quiescently for a minimum of 5 hours without disturbance. The as-prepared samples were maintained undisturbed at room temperature until required for characterisation measurements.

2.3 Polarised Optical microscopy (POM)

Optical microscopy images were recorded at 10× and 20× magnification with an Axio Scope A1 fluorescence microscope (Zeiss, Jena, Germany) equipped with Axiocam 105 colour camera. Polariser and analyser crossed at 90° were used for collecting POM images. To minimise shear flows which could lead to crystal aggregate break up, the material was slowly transferred from vessel to a glass microscope slide using a spatula. A coverslip was gently then placed over the sample and the images acquired. Zen Lite 2014 software was used to operate the instrument, and ImageJ was used to process and convert the collected images [42].

2.4 X-ray scattering

SAXS measurements of anhydrous SDS powder, SDS mixtures with glycerol and/or water, analogous *n*-alkyl sulfate mixtures and isothermal crystallisation of SDS mixtures were performed on a Xenocs Xeuss 2.0 SAXS laboratory beamline equipped with a metal jet X-ray source (GaK_α-radiation, wavelength of X-ray radiation $\lambda = 1.3414 \text{ \AA}$) (Excillum, Kista, Sweden), and Pilatus 1M pixel detector (Dectris, Baden-Daettwil, Switzerland) using a transmission mode. SAXS patterns were recorded over a scattering vector length range of $0.02 \text{ \AA}^{-1} < q < 1.1 \text{ \AA}^{-1}$, where $q = \frac{4\pi}{\lambda} \sin \theta$ and θ is half the scattering angle. SAXS patterns of

sodium hexadecylsulfate in glycerol were recorded over a range of $0.06 \text{ \AA}^{-1} < q < 0.9 \text{ \AA}^{-1}$, using a Bruker Nanostar laboratory SAXS instrument (Bruker AXS, Karlsruhe, Germany) modified with GeniX 3D X-ray source (CuK_α -radiation, $\lambda = 1.5418 \text{ \AA}$) and motorized collimating scatterless slits (Xenocs, Grenoble, France). For both apparatuses, q was calibrated using silver behenate powder. Two-dimensional (2D) SAXS patterns were transformed into one-dimensional (1D) curves by an azimuthal integration (also called circle gathering) using software supplied with the instruments. Calibration of the SAXS patterns and background scattering subtraction were performed using Irena SAS macros [43] for Igor Pro [44].

2-mm-diameter borosilicate glass capillaries were used as sample holders (WJM-Glass Muller GMBH, Berlin, Germany) for the X-ray measurements. For the isothermal crystallisation SAXS measurements the sample temperature was controlled using a HFSX350-CAP capillary heating stage (Linkam Scientific, Tadworth, UK). Samples were initially heated to $60 \text{ }^\circ\text{C}$ (for SDS systems) or $100 \text{ }^\circ\text{C}$ (for the other n -alkyl sulfate systems) for 5 minutes to achieve thermal equilibrium in the dissolved state, before cooling at a rate of $30 \text{ }^\circ\text{C min}^{-1}$ to $20 \text{ }^\circ\text{C}$. The chosen approach for the sample preparation was effective for avoiding preferable orientation of the studied lamellar structures. The temperature was then held for a minimum of 120 minutes while SAXS frames were acquired over the length of 59 seconds, with a total cycle time of 60 seconds. After a period where the intensity of the ensuing Bragg peaks remained constant, the measurement was ceased.

Solid content of SDS in glycerol mixture was also analysed using WAXS. The mixture was centrifuged at 4500 rpm for 15 minutes, with the supernatant decanted and discarded. The resulting pellet was then added to a paste cell and measured on a D8 ADVANCE X-ray diffractometer (Bruker AXS, Karlsruhe, Germany) (CuK_α -radiation, $\lambda = 1.5418 \text{ \AA}$) for 1.5 hours in a range of $1.2^\circ < 2\theta < 50^\circ$ using Bragg-Brentano geometry. Bruker Diffrac software supplied with the instrument was subsequently used to remove the amorphous scattering background.

2.5 Reconstruction of electron density distribution from SAXD

For a one-dimensional periodic lamellar structure, a projection of the ED distribution on the layer normal at a point z can be expressed as a Fourier series:

$$P(z) = \frac{1}{L} \sum_{l=-\infty}^{\infty} F(l) \cdot e^{-2\pi i \frac{lz}{L}} \quad (1)$$

where $F(l)$ is a structure factor (a Fourier term of the series) corresponding to a particular Miller index l and L is the lamellar period along the layer normal. Since $F(L)$ and $F(\bar{L})$ should be conjugate quantities the eq (1) could be rewritten in the form:

$$P(z) = \frac{1}{L} \cdot [F(0) + 2 \cdot P'(z)] \quad (2)$$

where

$$P'(z) = \sum_{l=1}^{\infty} |F(l)| \cdot \cos\left(\frac{2\pi lz}{L} - \delta(l)\right) \quad (3)$$

where $|F(l)|$ is the structure factor amplitude. Since n -alkyl sulfate molecules form crystal structures by packing in bilayers, the ED projection on the layer normal is expected to be symmetrical with respect to the layer center. For a structure possessing a symmetry centre, or a plane of symmetry, or a rotation (screw) axis parallel to the lamellae, the phase angle, $\delta(l)$, could be equal to either 0 or π . In this case eq (3) can be simplified further to:

$$P'(z) = \sum_{l=1}^{\infty} m(l) \cdot |F(l)| \cdot \cos\left(\frac{2\pi lz}{L}\right) \quad (4)$$

where $m(l) = \frac{F(l)}{|F(l)|} = \pm 1$ is the phase sign coefficient associated with a particular Miller index l .

$P'(z)$ represents the ED profile which is required for analysing the molecular packing along the layer normal. The structure factor amplitudes for eq (4) can be calculated from the corresponding total diffraction peak intensities, I_{00l} , of the lamellar structure:

$$|F(l)|^2 = \frac{I_{00l}}{LG} \quad (5)$$

where $LG = \frac{1}{\sin\theta \cdot \sin 2\theta}$ is the Lorentz-geometrical factor. Since the polarization factor is about 1 at small angles of diffraction, this factor has not been included in the calculations.

The diffraction peak intensities and position of n -alkyl sulfate-glycerol phases were obtained by fitting pseudo-Voigt functions using the Peak Analyser tool available in

Origin(Pro) 2020b [45]. Since the peaks belong to small-angle region of X-ray diffraction patterns, peak splitting caused by the K_{α} -doublet of characteristic X-ray radiation of chemical elements is insignificant and, therefore, it was neglected in the analysis. The periodic Bragg peaks of lamellar structures were identified for each sample in their SAXD patterns (see Supplementary Material, Figures S1-S5 and Tables S1-S5). The diffraction peak intensities obtained for the SDS systems were used to reconstruct projection of the ED profile on the layer normal for these systems (Figures S6-S8).

The Mercury (4.0) software program [46] was used to calculate structure factors for known anhydrous SDS crystal structure [47] in order to reconstruct and compare ED distribution along the SDS layer normal with the experimental data.

2.6 Avrami Kinetic data from SAXD data

The total intensity of selected diffraction peaks measured during crystallisation were analysed using the Johnson-Mehl-Avrami-Kolmogorov (Avrami) equation [48-52] to determine the nucleation and growth mechanisms of observed crystal phases [32,53-55]. A modified Avrami equation was used to account for the initial lag time [56]:

$$X_c = 1 - e^{-K(t-t_{ini})^n} \quad (6)$$

where X_c is the fraction crystallinity, K is the crystallisation rate constant, t is time, t_{ini} is the initial lag time of crystallisation and n is the Avrami exponent defined by the nucleation and crystal growth mechanism. In order to equate X_c to the fraction of crystallised species, the diffraction peak intensity of final (crystallised) products was scaled to unity.

3. Results and discussion

3.1 Visual and Microscopical observations of the SDS-glycerol gel phase

SDS is prevalent in a wide range of high volume, home, and personal-care consumer goods [57] and was the primary focus of this study. However, to aid the understanding of the underlying physical principles of its crystallisation, a range of homologous n -alkyl sulfates

were studied as well. It has also been found that heating a 2 wt% SDS in glycerol mixture (i.e. concentrations above the critical micellar concentration [13]) above the Krafft temperature followed by a subsequent quiescent cooling yielded a translucent phase that formed a freestanding gel. The transition from a clear micellar solution to translucent gel phase occurred over the course of 4 hours when the SDS in glycerol mixture cooled quiescently to room temperature (Figure 1A). Polarised optical microscopy of the gel phase revealed a network of birefringent, crystalline 'twisted ribbons' (Figure 1B). Further to this, all ribbons displayed a degree of curvature, with defined twists. This morphology is in stark contrast to the platelets and needles typically observed for anhydrous or hydrated crystals of SDS [32]. The formation of an entangled network of ribbons can be considered to be the cause of the gelation of the mixture, as observed within other microfibrillar (e.g. coagel) systems [22,36]. This corresponds to the observations of the phase described by Matthews *et al.* [15].

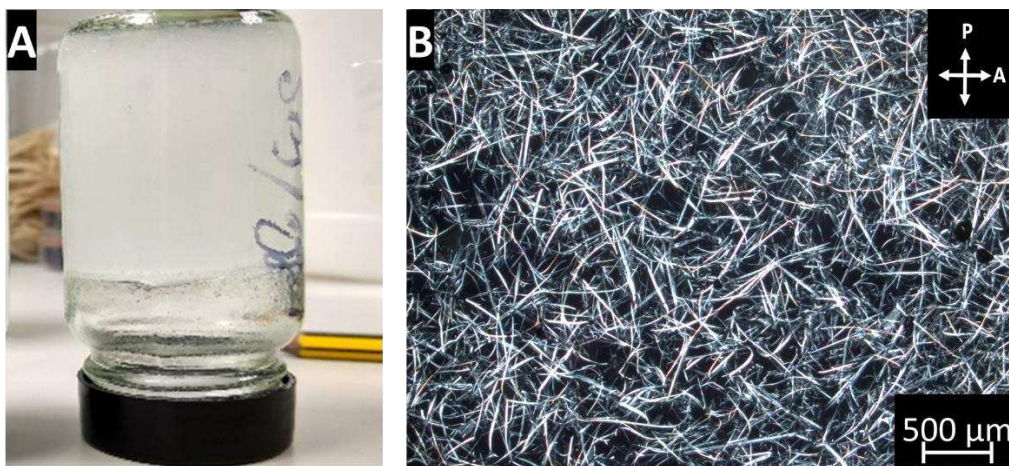


Figure 1. A) 2 wt% SDS in glycerol forming a free-standing gelled solution after heating to 60 °C and cooling quiescently to room temperature for 4 hours. B) Polarised optical microscopy image of the gelled 2 wt% SDS in glycerol. White arrows assigned by 'P' and 'A' show orientation of the polariser and the analyser plane, respectively.

3.2 Small angle x-ray scattering/diffraction analysis of SDS in glycerol

The SAXS pattern from a gelled 2 wt% SDS in glycerol mixture comprises a series of four prominent Bragg peaks at room temperature (Figures 2A and S2, and Table S2). The peak

position relationship suggests a lamellar structure, much like anhydrous SDS [47] (Figures 2B and S1, and Table S1). However, only the 1st, 2nd, 3rd, and 5th order peaks of the lamellar structure are present with the 4th order peak either very weak or absent. The d_{001} -spacing ($d_{001} = 2\pi/q_{001}$, where q_{001} is the 001 diffraction peak maximum position of the lamellar structure), corresponding to the lamella period, is calculated to be 55.1 Å (Table S2). In comparison, anhydrous SDS is known to have a d_{001A} -spacing of 38.9 Å [47] (also see Table S1). SDS molecule long axis (director) in the anhydrous crystals have a tilt of about 15° with respect to the layer normal, meaning the lamellar period is only 1.4 Å shorter than at a hypothetical 0° alkyl chain tilt. The change in d_{001} -spacing cannot, therefore, be solely the result of a change in SDS molecular tilt within the crystal. Consequently, it is highly likely that self-assembly between the glycerol and the SDS molecules has occurred upon cooling below the Krafft temperature of the mixture as proposed by Matthews *et al.* [15]. Considering the well-resolved sharp diffraction peaks (Figure 2A) which are analogous in their appearance to anhydrous SDS (Figure 2B) and other crystal structures formed by compounds containing *n*-alkyl chains [47,58–60], the observed pattern corresponds to a crystal phase comprising SDS-glycerol structural units.

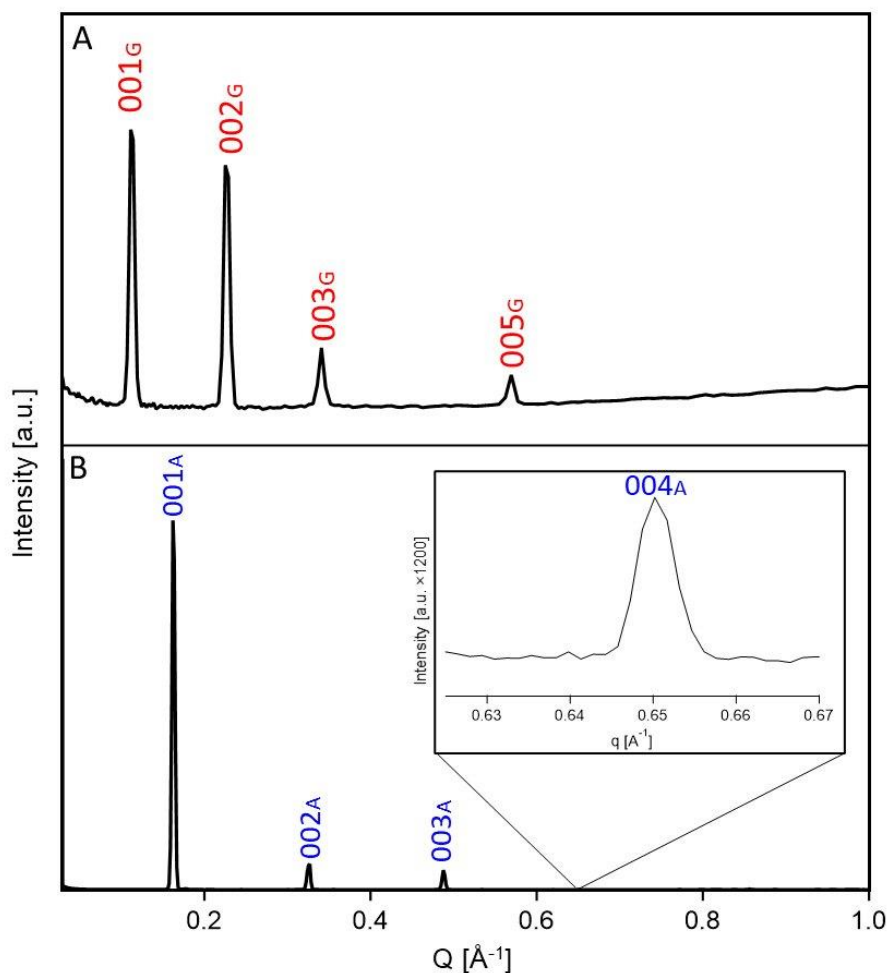


Figure 2. 1D SAXD pattern of A) gelled 2 wt% SDS in glycerol mixture and B) anhydrous SDS powder with inset showing 4th order diffraction peak, where 00_G and 00_A indicate lamellar peaks of SDS-glycerol and anhydrous SDS crystal phase, respectively. The observed diffraction peaks are assigned by Miller indices corresponding to a lamellar structure.

By using intensities and location of Bragg peaks within the experimental diffraction pattern of the SDS-glycerol crystal phase, it is possible to estimate the molecular packing along the layer normal using a Fourier transformation [61,62]. This method has been applied for the identification of packing of hydrocarbon molecules such as triacylglycerols [38]. Using the Fourier term series, represented by structure factor amplitudes calculated from the corresponding diffraction peak intensities, the ED profile along the layer normal of the lamellar structure can be determined [equations (2)-(5)]. In doing so, a location of different molecular components populated with heavier (high ED) and lighter (low ED) atoms can be detected. For SDS the sulfate head group can be identified as having a higher ED than that of an alkyl chain (tail), furthermore any co-ordinated species, such as glycerol molecules, could

also be recognised within the layer structure. The resolution of this method is dependent on the quantity of reflections [the number of Fourier terms, eq (5)] available from the experimental pattern for calculating $P'(z)$ using eq (4).

In order to reconstruct ED profile using eq (5), phase signs of the Fourier terms, $m(l)$, should be defined. In the case of the anhydrous SDS and the potential SDS-glycerol crystal phase, four non-zero intensity reflections (Figures 2, S1 and S2), hence $|F(l)|$, generate sixteen ($= 2^4$) possible variants of assignment. To resolve the problem of the phase assignment for the Fourier series from the proposed crystal phase, the ED profile results were interpreted within the context of anhydrous SDS, as this is a known structure [47]. Both structure factor amplitudes measured from experimental SAXD data (Figures 2B and S1) and calculated from atomic positions of anhydrous SDS crystals, subjected to a Fourier transform (Figures S6 and S7, respectively), yield ED profile projections on the layer normal (Figure 3). Herein, the $m(l)$ phase signs of the known SDS crystal structure were used for the corresponding Fourier term amplitudes calculated from the experimental anhydrous SDS patterns (Figure 2B). On comparing both datasets, the main structural features of the ED profile for experimental and simulated peak data were seen to be similar (Figure 3D and Figure 3C, respectively). Two prominent maxima representing the head groups, as well as two minima representing a lower region of electron density, can be identified in both profiles. The cause of this is the differing atomic composition, in which the headgroup contains sulfur (and oxygen and Na^+), heavier than the carbon and hydrogen constituents of the tail group. Nevertheless, there are small differences in intensities for experimentally derived and simulated ED profiles. A possible reason for this could be high levels of structural imperfections occurring in the SDS packing formed during crystallisation in contrast to an equilibrated crystal structure with a low level of defects usually used for crystal structure determination. This should also be considered when comparing SDS crystal phases, as minor fluctuations in ED may be seen in the alternate density profiles.

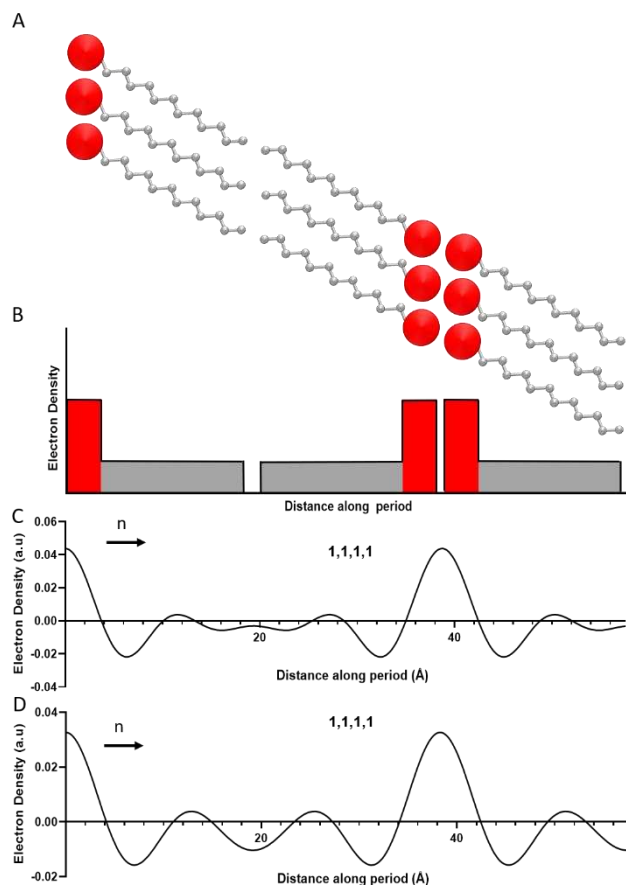


Figure 3. A) Packing of SDS molecules in an anhydrous crystal along the layer normal. B) Schematic of electron density (ED) distribution highlighting the SDS atomic composition along the layer normal. C) Projection of the ED profile on the layer normal, indicated by vector \mathbf{n} , reproduced from corresponding structure factors calculated for crystalline anhydrous SDS [47]. D) Projection of the ED profile on the layer normal, indicated by vector \mathbf{n} , calculated from the experimental SAXD data of crystalline anhydrous SDS (Figure 2A). The set of numbers at the top of each ED profile shows $m(l)$ coefficients representing the Fourier term phase signs for all four structure factor amplitudes observed in the SAXD pattern.

The head and tail motifs identified for the anhydrous crystals have been used to inform a structural model which describes the SDS-glycerol crystal structure in one dimension. By applying a Fourier transformation to the structural data gained from the SAXD patterns of the SDS-glycerol crystal phase, several possible ED profiles (Figure S8), generating the same diffraction peaks, can be produced. However, the one selected (Figure 4A) matches best the ED profile of the SDS molecules as seen in anhydrous SDS crystals (Figure 3D). The majority of the profile displays a similar morphology to that of anhydrous SDS. Large maxima represent the sulfate head groups (as indicated by H_1 and H_2 in Figure 4A), with a region of

lower electron density in between representing the *n*-alkyl chains. However, unlike anhydrous SDS, where the adjacent head groups are represented by a single broad peak (Figure 3), the SDS-glycerol phase shows two peaks separated by a gap with a unique region of the ED profile (indicated by a letter "G" in Figure 4A). This gap could correspond to a glycerol sublayer complexed within the SDS crystal and can be estimated to have a maximum thickness of 7 Å. Although the measured value should include a degree of inter-molecular spacing between glycerol and SDS molecules. Another difference between the SDS-glycerol crystal phase and anhydrous crystal ED profile is the representation of the polar head groups. For anhydrous SDS, the halfwidth of the terminal region represents a single head group. Conversely, for the SDS-glycerol crystal phase, it might be expected that the whole peak width is a closer representation of a single head group. Nevertheless, the halfwidth of the reconstructed head group peaks are similar for both structures. It is thought that due to limited number of Fourier terms available from the experiment, 4 diffraction peaks, the head groups convoluted by other atoms are not well resolved. Future work aimed for growing equilibrated SDS-glycerol crystals with small number of defects, possibly generating diffraction patterns containing higher order reflections, could allow improved resolution of the ED profiles to be obtained.

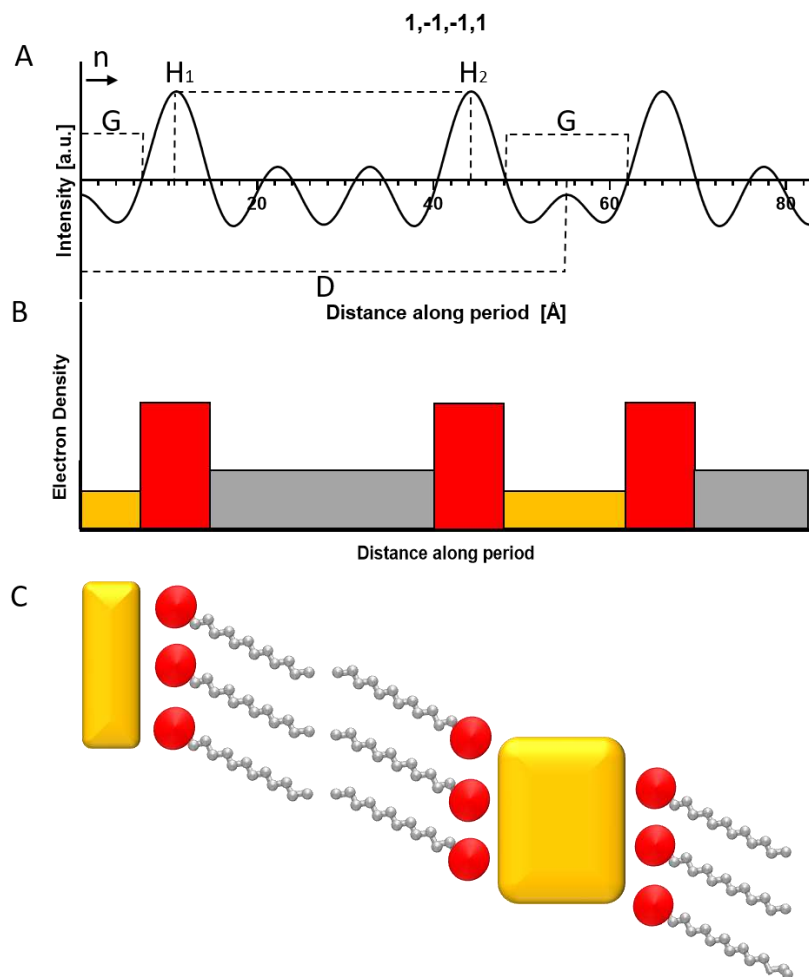


Figure 4. A) The most suitable projection of electron density (ED) profile on the layer normal, indicated by vector \mathbf{n} , reconstructed from experimental SAXD lamellar peaks of SDS-glycerol crystal phase (Figure 2A), with the distance between H_1 and H_2 representing the head-to-head spacing, G indicates the region containing glycerol and D indicates the structure period (d_{001} -spacing). The set of numbers at the top of the profile shows $m(l)$ coefficients representing the Fourier term phase signs for all four structure factor amplitudes observed in the SAXD pattern. B) Schematic of the ED distribution relating the position of SDS components [head group (red) and hydrocarbon tail (grey)] and glycerol (yellow) along the SDS-glycerol layer normal. C) Packing of SDS (coloured by red and grey) and glycerol (yellow) molecules along the layer normal where glycerol lies approximately in the yellow area.

By considering the sulfur atom to be the centre of the head group, tilt angle of SDS molecules with respect to the layer normal can be estimated using the projection of ED profile. This does not consider additional off-projection-plane tilt, which could be expected at small magnitudes, just like it is for anhydrous SDS. However, this additional minor tilt should not significantly influence the overall spacing estimates. In a single molecule of SDS, the

known distance from sulfur to the furthest terminal hydrogen on the alkyl chain is 17.5 Å [47]. Furthermore, length of a projected distance between the terminal hydrogen atoms of adjacent SDS molecules in the bilayer onto the molecular long axis, is about 0.5 Å. Assuming a similar inter-SDS spacing in the SDS-glycerol crystal structure, a theoretical maximum distance between the sulfur headgroups is expected to be 35.5 Å (corresponding to a zero tilt of SDS molecules). In comparison, the distance between two maxima associated with SDS packing in the SDS-glycerol bilayer (Figure 4C, maxima indicated by H₁ and H₂) is 33.3 Å. Considering the theoretical maximum distance at zero tilt, an estimated tilt of SDS molecules with respect to the layer normal in the SDS-glycerol crystal structure is about 20°, which is reasonably close to the SDS tilt of 15° in the anhydrous SDS crystal structure.

According to the ED profile, the distance between two SDS head groups, separated by glycerol inclusions, projected on the layer normal is about 21.6 Å. This distance should be composed of an SDS head group diameter of approximately 4 Å (estimated from a projection of the sulfur-to-sulfur distance of adjacent SDS heads) with the remaining 17.8 Å taken up by SDS-glycerol and glycerol-glycerol inter-molecule distance projections. On measuring the longest distance between hydrogens of terminal alcohol groups in glycerol, giving an approximation for the molecule length [63], a 5.6 Å distance could be found. Assuming that there are two glycerol molecules lie parallel to the layer normal and the inter-molecular distances are about 2 Å, the total length can be estimated as 17.2 Å which is close to the expected value of 17.8 Å. However, a better resolution of the ED profile would be desirable, as the spacing information deduced in this study alone (Figure 4C) is not sufficient to make a more definite conclusion. Considering the elemental composition and mass density of glycerol, it would be expected that the maxima in the ED profile corresponding to the glycerol region would be higher than the SDS alkyl chain at equimolar ratios [64,65]. In this respect, it should be suggested that glycerol is present in amounts slightly lower than the equimolar stoichiometry.

By relating the ED profile (Figure 4C) to the microscopy data (Figure 1B), it is possible to rationalise some aspects of the ribbon structure seen using POM. One notable feature is the

ribbon twisting. Since no chiral centre is present, SDS is an achiral molecule whereas glycerol is prochiral, the twist is unlikely to have a microstructural origin within the unit cell [66], even though it could not be fully ruled out. One of possible causes for the twist formation, much like in polymer crystallisation, could be a stress on a bilayer stack produced by spontaneous unbalanced growth [67].

3.3 Wide angle x-ray scattering/diffraction analysis of SDS in glycerol

WAXS from a 2 wt% SDS-glycerol crystal phase yielded low intensity peaks at $2\theta > 10^\circ$ due to the scattering from amorphous (liquid) glycerol dominating the pattern. Therefore, to increase sensitivity in the wide angle region, an 8 wt% solution of SDS was subsequently prepared and centrifuged to remove the majority of bulk glycerol. Nevertheless, the resulting scattering pattern still exhibited a pronounced diffuse peak shape (Figure S9). This peak appears to be similar to the peak in a scattering pattern of liquid glycerol (Figure S10), suggesting there is a substantial amount of liquid/bulk glycerol remaining in the centrifuged 8 wt% SDS in glycerol mixture. Thus, scattering of the amorphous component observed in the centrifuged solution scattering pattern (Figure S9) has been subtracted using the liquid glycerol WAXS pattern (Figure S10). The resulting pattern (Figure 5) at small angles displayed peaks similar to SAXD of 2 wt% SDS in glycerol mixture (Figure 2A) (albeit the relatively low intensity of 001_G peak affected by air scattering and the diffractometer resolution at small angles), indicating that the phase composition of the SDS-glycerol system remains similar at higher SDS concentrations. Furthermore, high concentration of the SDS-glycerol crystal phase in the centrifuged sample enabled very weak 4th and 6th order lamellar peaks to be detected (Figure 5, left inset).

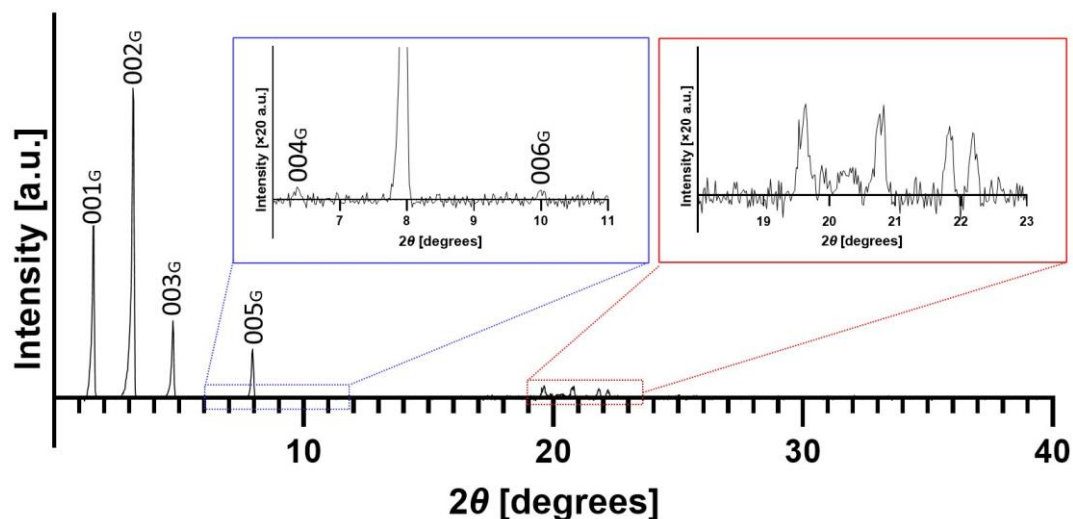


Figure 5. Background corrected WAXD patterns of centrifuged 8 wt% SDS in glycerol mixture ($\text{CuK}\alpha$ -radiation). The left inset (blue rectangle) and the right inset (red rectangle) show low-intensity lamellar peaks and characteristic fingerprint region of SDS-glycerol crystal phase.

The diffraction pattern has also demonstrated a set of well-defined peaks in the region of $18^\circ < 2\theta < 23^\circ$ (Figure 5, right inset) which, in terms of location, are analogous to anhydrous SDS [47] and related to a position of reflections associated with a sub-cell formed by packed *n*-alkyl chains [68]. Alkyl chains oriented parallel to the layer normal can form a hexagonal sub-cell, classified as a rotator phase, producing in this region of diffraction pattern a single 100 (hexagonal) peak corresponding to d -spacing $\sim 4.1 \text{ \AA}^{-1}$. Furthermore, frozen rotational motion of the alkyl chains around their axis causes a directional orientation of the zigzag planes of the hydrocarbon chains and a reduction of the hexagonal sub-cell to an orthorhombic sub-cell typical for many alkanes such as polyethylene producing two pronounced 110 and 200 orthorhombic peaks corresponding to $d \sim 4.2 \text{ \AA}^{-1}$, and $d \sim 3.7 \text{ \AA}^{-1}$, respectively [69]. An additional tilt of the acyl chains to the layer normal due to an arrangement of the terminal methyl groups within the inter-layer space produces a set of peaks associated with a monoclinic or triclinic sub-cell [68]. The latter is likely to be the case for the SDS-glycerol crystals demonstrating at least four peaks in the WAXD region (Figure 5, the right inset). Thus, both the ED profile (Figure 4) and the WAXD results indicate that acyl chains of SDS are tilted with respect to the layer normal.

SAXD and WAXD data (Figures 2A and 5) indicate a highly ordered structure through multiple diffraction peaks, with scattering patterns akin, for example, to crystalline fats [54]. Furthermore, POM indicates large birefringent aggregates rather than nanosized assemblies. The SDS within the ribbon phase can, therefore, be considered highly ordered and crystalline. However, as the crystal structure has not been fully solved, it is not possible to verify the degree of crystallinity in the glycerol layer. Matthews *et al.* describe the system as paracrystalline [15]. Nevertheless, a high degree of long-range order, demonstrated by relatively sharp diffraction peaks observed in SAXD region and, in particular, WAXD region suggests that the SDS-glycerol phase has to be a crystalline phase.

3.4 Co-crystallisation of *n*-alkyl sulfate homologues in glycerol

The literature suggesting that self-assembly is mediated via interactions with the head group can be further tested through formation of analogous species with the same head group moiety [70,71]. A series of homologous *n*-alkyl sulfate surfactants with even chain lengths ranging from C10-C18 were studied to detect whether self-assembly with glycerol took place in a similar manner. One notable deviation from the original procedure was that during the thermal cycle all samples were heated to 100 °C (as opposed to 60 °C) to allow for full dissolution. Even chain length surfactants were chosen to maintain the geometry of methyl terminal packing of the molecules. It was seen that upon quiescent cooling to room temperature, the C10 surfactant mixture remained soluble producing a homogenous, clear solution. However, gelation was observed in mixtures of glycerol and surfactant with chain length in the range C12-C18. In an analogy to the SDS (C12 surfactant) (Figures 1A and S11A), optical microscopy observations indicate evidence of ribbons in the C14 and C18 surfactants (Figures S11B and S11C, respectively). Unfortunately, for the C14 and C18 surfactants only mixed phases (represented by ribbons, platelets, and needles) were observed. Furthermore, for the C16 surfactant, with the highest impurity level, it was not possible to distinguish individual crystals.

SAXS measurements of the C14-C18 *n*-alkyl sulfate gels confirmed the presence of hydrated and anhydrous surfactant crystals alongside the crystal phase containing glycerol (Figures S3-S5). This mixed phase composition is likely due to impurities such as synthetic precursors, the presence of water and, more importantly, an admixture of surfactants with other acyl chain lengths which could affect the main chain packing and distort the long-range lamellar structure. In a comparison with the SDS-glycerol crystal phase (Figure 2A), the lamellar diffraction peaks associated with the C14-C18 surfactant-glycerol phase (Figures S3-S5) are shifted to lower q -values. This should be expected because the bilayer was elongated through the added carbons in the surfactant hydrocarbon tail. d_{001} -spacing (period of the lamellar structure) plotted against the number of carbons in the alkyl chain for the surfactant homologous series demonstrated a linear trend with an average increase of 5.4 Å per pair of carbon atoms added to the chain (Figure 6). Considering the bilayer packing motif of the chains, this should correspond to 1.35 Å per carbon which is consistent with a length of projection of the bond between two carbon atoms of an alkyl zig-zag chain on the molecule director equal to about 1.3 Å [72].

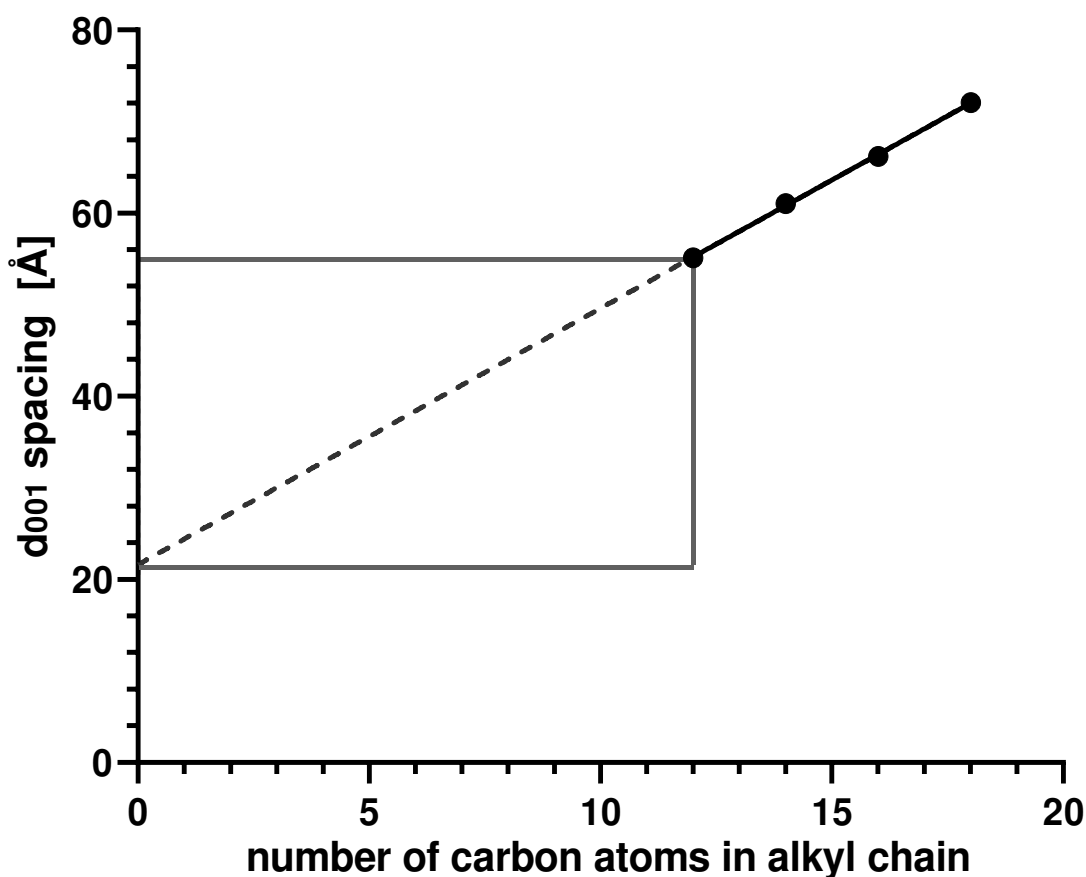


Figure 6. Period of lamella (d_{001} -spacing) measured from SAXD patterns of n -alkyl sulfate surfactants in glycerol mixtures homologous series versus number of carbons in the surfactant hydrocarbon tail. Linear regression is extrapolated to the theoretical '0 carbon in chain' for an n -alkyl sulfate molecule exhibiting an n -alkyl sulfate-SDS crystal phase.

The linear trend observed for d_{001} -spacings of the homologous series enables thickness of a sub-layer to be measured. The sublayer is comprised of sulfate head groups, glycerol, and the intermolecular distance between adjacent surfactant molecules. Indeed, an extension of the trend line to a point corresponding to a zero number of atoms per acyl chain should correspond to the thickness of the remaining sub-layer, which is calculated to be 21.6 Å (Figure 6). The obtained value is in an uncanny agreement with the sub-layer thickness estimated from the ED profile of SDS-glycerol crystal structure (21.6 Å) (Figure 4A).

Nevertheless, a minor disparity between the two measurements of the glycerol sublayer is observed, as the equal sublayer distance may represent different compositions. Assuming that the highest peak maxima of the ED profile correspond to the atomic position of sulfur,

the sublayer thickness calculated from this measurement should consist of a sulfate head group, glycerol and associated intermolecular distances. However, spacing information derived from the homologous series (Figure 6) should represent two headgroups, glycerol and the intermolecular distances. The latter suggests that the glycerol sublayer could be marginally thinner than it was estimated from the ED profile and, as a result, the originally calculated acyl chain tilt with respect to the layer normal could be slightly less than 20°. Despite the small ambiguity in regard to the sublayer depth observed, the correlation between the sublayer thicknesses measured by two independent methods strongly supports the set of Fourier term phase signs selected for the ED reconstruction of SDS-glycerol crystals (Figures S8 and 4A). In order to fully satisfy atomic positions, and hence sublayer thickness, a single crystal must first be obtained and analysed, which is beyond the scope of this work.

Comparing structural parameters of the SDS-glycerol phase measured in this work and recently published in literature [15] (Table 1), it can be concluded that both studies show similar results for the phase lamellar period and the glycerol sublayer. However, the phase composition determined in both works differs (Table 1), as the previous work estimates a value based only on the glycerol layer thickness, while the present study refers to the ED profile along the layer normal reconstructed from diffraction data. The latter also enables the acyl chain tilt to be measured (Table 1). In addition, WAXS data collected in this work (Figure 5) points to crystalline nature of the SDS-glycerol phase. By determining a ubiquitous glycerol sublayer depth through the lamellar period regression, structural information can be inferred for the observed *n*-alkyl sulfate-glycerol homologue crystal phases (Table 1), although with a lower degree of certainty than methods utilising ED profiles. The present work advances the initial findings [15], suggesting the phase is more akin to crystalline materials, such as coagels, than a paracrystalline mesophase. These results have implications for physical and applicative properties including crystallisation temperature and rate.

The study shows that the co-crystallisation of even-chained *n*-alkyl sulfates with glycerol is independent of the tail length and geometry. This is not surprising considering the relevant literature on ascorbate surfactant coagelation [73,74]. Multiple authors have reported high

aspect ratio co-crystals in the presence of water, with varying tail geometries ranging from single to double chains [29,30,34,74]. This suggests that surfactant self-assembly is highly dependent on head group and packing.

Table 1: Comparison of structural parameters identified in the current work and previous literature for the *n*-alkyl sulfate-glycerol crystal phase.

	SDS (C12)		C14	C16	C18
Source of information	Matthews <i>et al.</i> [15]	This work	This work	This work	This work
Lamellar period [Å]	55.6	55.1	61.0	66.2	72.1
Thickness of glycerol region including intermolecular spacing [Å]	8	7 ^{#†}	7 [†]	7 [†]	7 [†]
Molecular tilt [degrees]	N.A.	20 ^{#†}	20 [†]	20 [†]	20 [†]
Glycerol: SDS stoichiometry	1.5-2.0	≤1:1 [†]	-	-	-
Phase characterisation	Paracrystalline mesophase	Co-crystal	Co-crystal	Co-crystal	Co-crystal

[#] Estimated through determination of sublayer region within the electron density profile reconstructed from diffraction data

[†] Estimated through sublayer depth of *n*-alkyl sulfate homologues, Sublayer values and tilt represent maximum values due to limitations in determining intermolecular spacing within the sublayer.

3.5 Effect of water on the SDS-glycerol phase formation during isothermal cooling

Given that highly structured solutions of the SDS-glycerol crystal phase can be readily observed macroscopically and that their self-assembly is of considerable commercial interest as structuring agents in commercial cleaning products, one question remains, why have they not been intensively studied and reported in the literature? Could it be due to the inhibition of structure formation by composition or environmental factors? The most important factor influencing the formation of *n*-alkyl sulfate-glycerol crystals is water, the hygroscopic nature of both glycerol (a humectant) and SDS (a salt) create an environment where water is almost always present and interferes with the co-crystallisation [6,75–77]. To test this, 2 wt% SDS (total weight) in glycerol-water mixtures were prepared in the same manner as the SDS-glycerol gels. It was found by using optical microscopy that platelet/needle crystals formed

alongside ribbons of the SDS-glycerol crystal phase when solutions with only 2.9 wt% of the total solvent content being water were cooled quiescently (Figure 7A). The presence of multiple morphologies was superseded by pure platelet/needle above 5 wt% water content (Figure 7B), with morphologies similar to anhydrous SDS [73]. Beyond this water content, non-ribbon crystals were the predominant species.

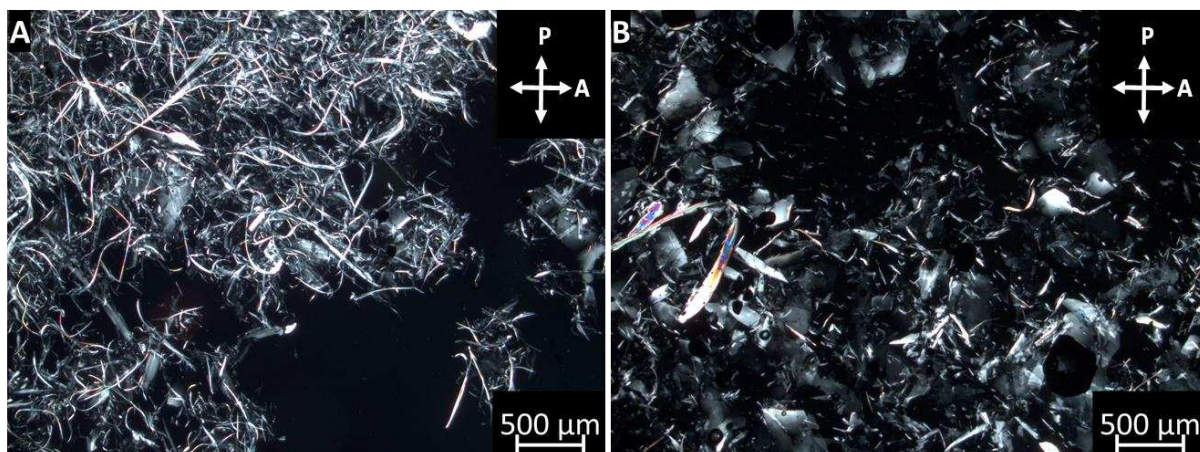


Figure 7. Representative polarised optical microscopy images of A) the mixed phase containing platelet, needle and ribbon crystal phases formed after heating and cooling of a 2 wt% SDS solution in a water-glycerol mixture with a water content of 2.9 wt% of the solution, B) platelet and needle crystals formed after heating and cooling of a 2 wt% SDS solution in a water-glycerol mixture with a water content of 5.6 wt% of the solution. White arrows assigned by 'P' and 'A' show orientation of the polariser and the analyser plane, respectively.

Isothermal cooling of 2 wt% SDS in water-glycerol mixtures was subsequently studied at 20 °C using time-resolved SAXS to determine the effect of water on the crystal formation (Figures S12-S17). Time-resolved diffraction peak intensities and positions were obtained using the Multi-peak Fit procedure within the Irena SAS macros [43] available for Igor Pro 8 software [44]. The periodic Bragg peaks of lamellar structures were identified for each sample in their SAXD patterns. In mixtures containing water, two sets of lamellar peaks are observed in SAXD patterns (Figure 8, inset), indicating a formation of two separate structures, one of which corresponds to the SDS-glycerol crystal phase. The other structure formed is anhydrous SDS crystals. This is indicated by the diffraction peak corresponding to d -spacing of about 39 Å similar to the literature d_{001} value of SDS crystals [47], as well as to the results

presented herein for an SDS powder (Figures 2B and 1S). The intensity of the SDS-glycerol crystal diffraction peaks reduces with increasing amounts of water until disappearing completely in a solvent comprising 5 wt% water (Figure 8). This is in a stark contrast to literature data suggesting hydrate crystals to be formed in water-glycerol mixtures [10,13].

To quantify the relative abundance of each species, the d_{001} peak intensity of each phase was measured during and after the requisite cooling period. 2D SAXS patterns revealed that the SDS anhydrous crystal phase produced anisotropic spotted diffraction rings (Figure S18) indicating that large and textured crystals were formed. The intense spot-like reflections, associated with these large, oriented crystals, were slightly displaced from their angular positions due to geometrical aberrations, manifested in an uneven distribution of peak intensity in the integrated 1D diffraction patterns (Figure 8, inset) and its fluctuation with time. To offset this effect, a time-average value was taken for the plateau intensity of the d_{001} peak recorded during the isothermal cooling (Figures S12-S17). Therefore, the diffraction peak intensity fluctuation originating from the crystal growth and movements were minimised. The relative average peak intensities plotted against the water content demonstrates a sigmoidal change over a very small increase of water in the solvent composition (Figure 8). This suggests an active disruption of the SDS-glycerol crystallisation process by water.

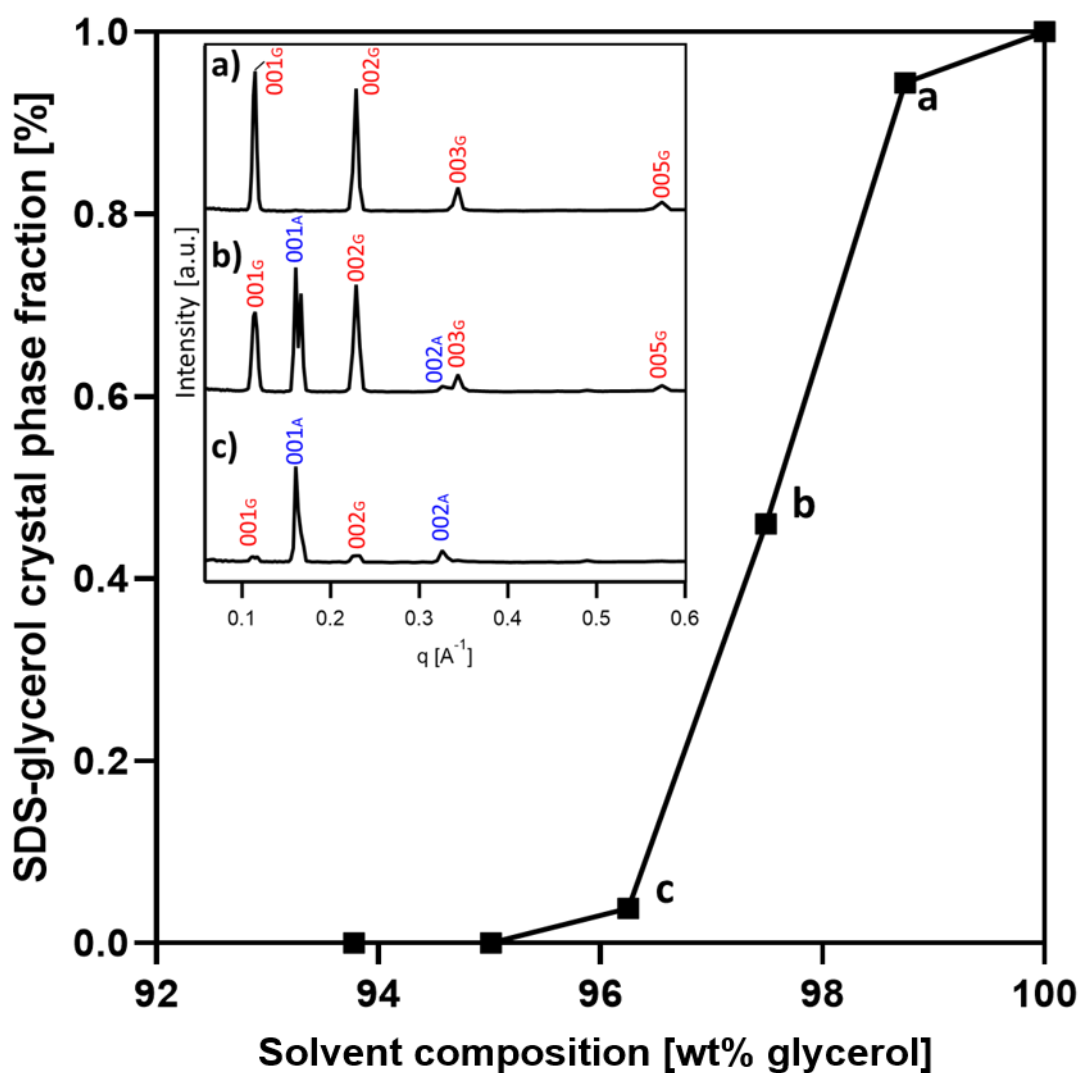


Figure 8. The dependence of relative SDS-glycerol crystal phase content (with respect to anhydrous SDS crystal phase content) on the glycerol concentration in glycerol-water solvent calculated from corresponding averages of 001_G and 001_A diffraction peak intensity observed in SAXD patterns of 2 wt% SDS in glycerol water solutions during isothermal cooling at 20 °C (Figures S12-S17). The inset contains selected representative SAXD patterns where $00l_G$ and $00l_A$ indicate lamellar peaks of SDS-glycerol and anhydrous SDS crystal phases: a), b) and c) correspond to representative frames obtained during isothermal cooling of mixtures containing 98.7 wt%, 97.5 wt% and 96.2 wt% glycerol in the solution, respectively.

More perplexing is why anhydrous crystals form in preference to the hydrate, as described by the literature [13]. Evidence of crystal polymorphism at different water-glycerol ratios is observed in the form of the varying suspension morphology in Abdel-Rahem's work [11]. A homogenous gel, similar to the SDS-glycerol crystal phase, is formed in a solution containing more than 91 wt% glycerol. Whereas separated inhomogeneous suspensions exist in

solutions with 45-90 wt% glycerol. However, due to the change in liquid density across the concentration range and different processing conditions, this information is not wholly comparable with the results presented here. Miller *et al.* indicate that in aqueous mixtures of SDS higher temperatures of crystallisation lead to higher hydration states and a formation of the large octagonal platelet morphology [32,33]. However, in this tertiary system, both the hydrophilic head of SDS and glycerol are likely to exhibit strong attraction to water, evidenced by their high degree of miscibility, the formation of hydrate SDS crystals, and a low water activity in a presence of glycerol, originating from polar non-covalent bonding seen in binary aqueous mixtures [64,78,79]. Agreeing with this, Khan *et al.* indicates a strong hydrogen bonding network between water, sulfate groups and glycerol in the same ternary systems [13]. Therefore, when water is present, it is likely that co-ordination of glycerol to the head group of SDS is inhibited, leading to tail organisation and nucleation. This 'tail-directed' crystallisation is in competition with the 'head-directed' organisation needed for the SDS-glycerol crystal phase to form.

The question is, however, where is the water located preceding to and hence during the phase transition? In this respect, two alternative hypotheses could rationalise the crystallisation behaviour. The conventional wisdom is that when SDS forms micelles in glycerol-water mixtures the SDS head group could be preferentially surrounded by water. This prevents glycerol from complexing to SDS and would further explain why competing crystallisation occurs: likely acting as a function of micelle surface area. However, if this were true, it would be expected that hydrates are more likely to form due to proximity to the sulfate headgroup. Furthermore, measurements by Ruiz *et al.* on micellar solutions of SDS in glycerol-water mixtures, suggest incorporation of glycerol within the solvent layer [80]. This is evidenced by increasing micro viscosity of the micelle surface as glycerol content is increased, and casts doubt on the hypothesis proposed above. An alternative explanation is that the water is dispersed uniformly as single molecules or in the small clusters seen in glycerol-water binary mixtures [79,81]. There is abundant literature [82-85], both experimental and theoretical, that demonstrate that the activity of water is suppressed in

admixture with glycerol, most likely due to H-bonding, with an activity coefficient that is much smaller than 1 in the concentrations of interest. This accounts for the formation of the anhydrous crystals at low water content, and the water is retained in the liquid phase. From a molar perspective there is far more glycerol than surfactant to tie-up the water due to interactions occurring when glycerol becomes 'hydrated' with water [86]. Why this also prevents glycerol from binding to the SDS head group needs further study, it could be that the corollary reduction in the activity of glycerol made the anhydrous phase to become the equilibrium structure. Further studies must be conducted to determine more aspects to this phenomenon, nevertheless the experimental results show the sensitivity of SDS to glycerol-water systems.

Analysis of crystallisation kinetics, including the mode and dimensionality of crystal growth, is also possible by using the Avrami equation [eq (6)]. The anisotropy and mosaicity within the obtained 2D SAXS patterns (Figure S18), especially for samples containing anhydrous crystals, meant that a comparison between the anhydrous and SDS-glycerol crystal phases was problematic in most cases. However, it was possible to obtain an isotropically averaged scan, and hence measure kinetic growth, using scattering data for 2 wt% SDS in glycerol. Furthermore, the sample containing the highest water content in the solution (6.3 wt%) exhibited minimal anisotropy, possibly due to a higher nucleation rate and, as a result, small crystals and aggregates. Therefore, this sample was used as a comparison to the crystal formation in pure glycerol. The data are plotted in the linearised double log to emphasise the unencumbered growth, and allowed determination of both the Avrami exponent and rate constant, which in turn informs the mode of growth (Figure 9) [54,55].

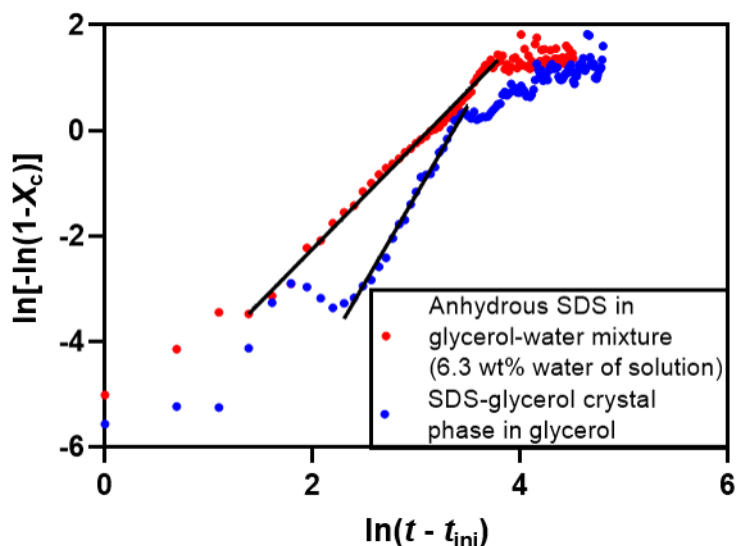


Figure 9. Linearised Avrami kinetic plot measuring crystal growth of SDS-glycerol crystal phase from 2 wt% SDS in glycerol (red) and anhydrous SDS crystals from 2 wt% SDS in glycerol-water (93.7 wt% glycerol and 6.3 wt% water in the solution) (blue), isothermally cooled at 20 °C and measured by time-resolved SAXS of d_{001} peak intensities (Figures S12, S17). The linear regressions (solid lines) equate to an Avrami exponent of 2.0 for SDS-glycerol phase and 3.4 for anhydrous SDS.

The Avrami exponent for SDS-glycerol crystal formation during isothermal cooling at 20 °C, determined through the gradient of linearised growth curves (Figure 9), yielded a value of 2.0. The result could be interpreted as a sporadic nucleation followed by 1D crystal growth, which is consistent with the large initial lag time [54] and the shape of the crystals formed. This is opposed to the other interpretation of an exponent of 2, spontaneous 2D crystal growth, which does not match the crystal aggregate dimensionality present in the microscopy data (Figure 1B). The convergence between the Avrami constant and expected integer values is noteworthy and suggests a uniform mode of growth occurring for the SDS-glycerol crystals. The anhydrous crystals formed in glycerol-water mixture yielded an Avrami exponent of 3.4 suggesting a mixed mechanism of crystal growth. Considering the majority formation of platelet type crystals expected (Figure 7B), 2D crystal growth type would be most likely, leading to an exponent of 2 or 3 depending on the nucleation mechanism. Spherulitic (three-dimensional) growth yields a constant of 3 or 4, depending on whether the nucleation is instantaneous or spontaneous and non-integer values of the Avrami exponent is often observed in polymer crystallisation [87]. As both needles and platelets are observed in

microscope images of this system (Figure 7B) a mixed growth might be expected. In general, the increase in both the rate and dimensionality of growth in the anhydrous SDS crystals with respect to the SDS-glycerol crystal phase may influence the kinetic favourability and be a contributing factor as to why it dominates in the presence of water.

4. Conclusions

The gel formed by SDS in glycerol, when cooled below the Krafft temperature, was shown to be a result of the formation of highly ordered SDS-glycerol crystal phase producing a microfibrillar morphology. The glycerol sublayer thickness of 7 Å measured for the glycerol-SDS crystal phase is in a close agreement with the value estimated by Matthews *et al.* [15]. However, the present analysis builds on the reconstruction of electron density profiles from lamellar diffraction peak intensities, which allows estimation of not only the SDS molecular tilt, approximately 20°, but also the sub-equimolar stoichiometry of glycerol within the phase to be estimated. WAXD data confirmed a presence of the tilt through the observance of a fingerprint pattern, indicating low-symmetry monoclinic or triclinic packing of the SDS alkyl chains [68], as well as giving insight into the crystalline nature of the phase.

For the first time, an analogous surfactant-glycerol co-assembly has been detected in even-chained *n*-alkyl sulfates with the carbon alkyl chain content from 12 to 18 atoms, where a periodic increase in lamellar spacing of 5.4 Å per pair of carbon atoms is observed. This clearly demonstrates a consistent structural surfactant-glycerol motif, and a uniform glycerol-sulfate layer thickness, defined by the sulfate-glycerol interaction. This finding is a pathway to future surfactant gel design and optimisation, with a potential to produce surfactant structuring systems with tuned physical properties such as gelation and/or crystallisation temperature.

A phase composition of SDS-glycerol-water ternary mixtures with water concentration below 6.3 wt% has been analysed. The SDS-glycerol crystal formation was shown to be inhibited by

water when the SDS-glycerol-water mixtures were cooled isothermally at 20 °C. Simultaneously, anhydrous SDS crystals were preferentially formed in these mixtures when the water content was increased, with the anhydrous phase dominating at water concentrations of 5 wt% and above. It is suggested that the competing interaction and hydration of glycerol by water, as opposed to SDS, are main drivers of this phenomenon, although a further study would be required. This contrasts with the hydrated crystals observed for SDS in glycerol-water mixtures in previous works [10-13], although expansion of the formulation range, and cooling temperature must also be considered in any further studies. The SDS-glycerol-water phase behaviour discovered in the present work increases applicable knowledge of the SDS-glycerol crystal phase, with implications for formulation and processing within industry due to the sensitivity to water. By understanding the crystal phase formation in this ternary system, a better control of rheology and surfactant activity can be achieved.

Declaration of Interests

The authors declare that they have no known conflicting financial interests or personal relationships that could have appeared to impact the work reported in this paper.

Acknowledgements

Unilever and UKRI are thanked for funding a CDT PhD iCASE studentship (EP/P510634/1) for J.C. O.O.M. thanks EPSRC for the capital equipment grant (EP/M028437/1) to purchase the laboratory-based Xenocs Xeuss 2.0/Excillum SAXS beamline used for characterizing the SDS/glycerol/water materials. The authors are grateful to Keith Owen for providing Karl Fisher measurement and Dr. Craig Robertson for collection of diffractometer data.

References

- [1] A. Kunal, S. Singh, *Glycerol Market Trends Analysis 2018-2024 World Industry Report*, 2018.
- [2] K. Pulidindi, H. Pandey, *Sodium Lauryl Sulfate Market Forecast Report 2019-2026*, 2019.
- [3] C. Edser, *Focus on Surfactants 2018* (2018) 1–2.
- [4] R. Ciriminna, C. Della Pina, M. Rossi, M. Pagliaro, *European Journal of Lipid Science and Technology* 116 (2014) 1432–1439.
- [5] M.M. Singer, R.S. Tjeerdema, in: *Reviews of Environmental Contamination and Toxicology*, Springer, New York, USA, 1993, pp. 95–149.
- [6] C.A.G. Quispe, C.J.R. Coronado, J.A. Carvalho Jr., *Renewable and Sustainable Energy Reviews* 27 (2013) 475–493.
- [7] Y. Sun, X. Li, Y. Deng, J.N. Sun, D. Tao, H. Chen, Q. Hu, R. Liu, W. Liu, X. Feng, J. Wang, M. Carvell, A. Joiner, *Journal of Dentistry* 42 (2014) S30–S38.
- [8] M.A. Zaman, G.P. Martin, G.D. Rees, *Journal of Dentistry* 36 (2008) 351–359.
- [9] Z. Lin, H.T. Davis, L.E. Scriven, *Langmuir* 12 (1996) 5489–5493.
- [10] R.A. Abdel-Rahem, *Journal of Dispersion Science and Technology* 34 (2013) 932–940.
- [11] D.J. Lee, W.H. Huang, *Colloid Polym. Sci.* 274 (1996) 160–165.
- [12] A. Zou, H. Hoffmann, N. Freiberger, O. Glatter, A. Makorsky, Y. Talmon, *Colloids and Surfaces A: Physicochemical and Engineering Aspects* 316 (2008) 226–233.
- [13] H. Khan, J. Seddon, R. Law, N. Brooks, E. Robles, J. Cabral, *Journal of Colloid And Interface Science* 538 (2018) 75–82.
- [14] E. Summerton, M.J. Hollamby, C.S. Le Duff, E.S. Thompson, T. Snow, A.J. Smith, C. Jones, J. Bettioli, S. Bakalis, M.M. Britton, *Journal of Colloid and Interface Science* 535 (2019) 1–7.
- [15] L. Matthews, Ż. Przybyłowicz, S.E. Rogers, P. Bartlett, A.J. Johnson, R. Sochon, W.H. Briscoe, *Journal of Colloid and Interface Science* 572 (2020) 384–395.
- [16] H. Hirata, N. Iimura, *Journal of Colloid and Interface Science* 199 (1998) 111–122.
- [17] J. Liang, Y. Ma, Y. Zheng, H. Ted Davis, H.T. Chang, D. Binder, S. Abbas, F.L. Hsu, *Langmuir* 17 (2001) 6447–6454.
- [18] C. V Nikiforidis, E.P. Gilbert, E. Scholten, *RSC Advances* 5 (2015) 47466–47475.
- [19] D.G. Cameron, H.H. Mantsch, *Biophysical Journal* 38 (1982) 175–184.
- [20] M. Tsuchiya, K. Tsujii, K. Maki, T. Tanaka, *J. Phys. Chem.* 98 (1994) 6187–6194.
- [21] R.P. Sperline, *Langmuir* 13 (1997) 3715–3726.
- [22] S. Palma, A. Jiménez-Kairuz, L. Fratoni, P. Lo Nostro, R. Manzo, D. Allemandi, *Farmaco* 58 (2003) 1271–1276.
- [23] S. Borsacchi, M. Ambrosi, P. Lo Nostro, M. Geppi, *Journal of Physical Chemistry B* 114 (2010) 15872–15878.
- [24] R.G. Weiss, *Journal of the American Chemical Society* 136 (2014) 7519–7530.
- [25] J. Raeburn, D.J. Adams, *Chem. Commun.* 51 (2015) 5170–5180.
- [26] Y. Lan, M.A. Rogers, *CrystEngComm* 17 (2015) 8031–8038.
- [27] M. Seth, L.G. Leal, *Journal of Rheology* 58 (2014) 1619–1645.
- [28] P. Lo Nostro, M. Ambrosi, B.W. Ninham, P. Baglioni, *Journal of Physical Chemistry B* 113 (2009) 8324–8331.
- [29] E. Carretti, V. Mazzini, E. Fratini, M. Ambrosi, L. Dei, P. Baglioni, P. Lo Nostro, *Physical Chemistry Chemical Physics* 18 (2016) 8865–8873.

- [30] E. Tempestini, M. Bucci, V. Mastromartino, M. Gori, D. Tanini, M. Ambrosi, E. Fratini, A. Capperucci, P. Lo Nostro, *ChemPhysChem* 18 (2017) 1400–1406.
- [31] X. Li, Y. Yang, Y. Qin, J. Dong, *Journal of Dispersion Science and Technology* 32 (2011) 465–469.
- [32] R.M. Miller, A.S. Poulos, E.S.J. Robles, N.J. Brooks, O. Ces, J.T. Cabral, *Crystal Growth & Design* 16 (2016) 3379–3388.
- [33] R.M. Miller, O. Ces, N.J. Brooks, E.S.J. Robles, J.T. Cabral, *Crystal Growth & Design* 17 (2017) 2428–2437.
- [34] M. Ambrosi, P. Lo Nostro, L. Fratoni, L. Dei, B.W. Ninham, S. Palma, R.H. Manzo, D. Allemandi, P. Baglioni, *Physical Chemistry Chemical Physics* 6 (2004) 1401–1407.
- [35] F.C. Wang, A.G. Marangoni, *RSC Advances* 4 (2014) 50417–50425.
- [36] S. Ogawa, M. Koga, K. Asakura, I. Takahashi, S. Osanai, *Journal of Surfactants and Detergents* 20 (2017) 255–261.
- [37] S. Palma, R.H. Manzo, D. Allemandi, L. Fratoni, P. Lo Nostro, *Langmuir* 18 (2002) 9219–9224.
- [38] O.O. Mykhaylyk, I.W. Hamley, *Journal of Physical Chemistry B* 108 (2004) 8069–8083.
- [39] K. Akabori, J.F. Nagle, *Soft Matter* 11 (2015) 918–926.
- [40] E. Summerton, G. Zimbitas, M. Britton, S. Bakalis, *Journal of Crystal Growth* 455 (2016) 111–116.
- [41] A. Okoampah, L. Tang, *Latin American Journal of Pharmacy* 34 (2015) 576–584.
- [42] C.A. Schneider, W.S. Rasband, K.W. Eliceiri, *Nature Methods* 9 (2012) 671–675.
- [43] J. Ilavsky, P.R. Jemian, *Journal of Applied Crystallography* 42 (2009) 347–353.
- [44] Igor pro 8, Wavemetrics, Lake Oswego, OR (<https://www.wavemetrics.com/products/igorpro> accessed June 27, 2020).
- [45] Origin(Pro) 2020b, OriginLab Corporation, Northampton, MA (<https://www.originlab.com/> accessed June 27, 2020).
- [46] C.F. MacRae, I. Sovago, S.J. Cottrell, P.T.A. Galek, P. McCabe, E. Pidcock, M. Platings, G.P. Shields, J.S. Stevens, M. Towler, P.A. Wood, *Journal of Applied Crystallography* 53 (2020) 226–235.
- [47] L.A. Smith, R.B. Hammond, K.J. Roberts, D. Machin, G. McLeod, *Journal of Molecular Structure* 554 (2000) 173–182.
- [48] M. Avrami, *The Journal of Chemical Physics* 7 (1939).
- [49] M. Avrami, *The Journal of Chemical Physics* 8 (1940) 212–224.
- [50] M. Avrami, *The Journal of Chemical Physics* 9 (1941) 177–184.
- [51] W.A. Johnson, R.F. Mehl, *Transactions of the American Institute of Mining and Metallurgical Engineers* 135 (1939) 416.
- [52] A. Kolmogoroff, *Izvestiya Rossiiskoi Akademii Nauk. Seriya Matematicheskaya* 1 (1937) 355–359.
- [53] M.S. Lisowski, Q. Liu, J. Cho, J. Runt, F. Yeh, B.S. Hsiao, *Macromolecules* 33 (2000) 4842–4849.
- [54] A.G. Marangoni, L.H. Wesdorp, *Structure and Properties of Fat Crystal Networks*, Second Edition, CRC Press, Boca Raton, 2013.
- [55] A.B. Matheson, V. Koutsos, G. Dalkas, S. Euston, P. Clegg, *Langmuir* 33 (2017) 4537–4542.
- [56] J. Lelito, *Materials*. 13 (2020) 2815.
- [57] <https://echa.europa.eu/substance-information/-/substanceinfo/100.005.263> (accessed June 27, 2020).
- [58] S.T. Reddy, K.P. Krovi, M.J. Swamy, *Crystal Growth & Design* 14 (2014) 4944–4954.

- [59] K. Takeda, Y. Andoh, W. Shinoda, S. Okazaki, *Langmuir* 35 (2019) 9011–9019.
- [60] J.K. Cockcroft, A. Shamsabadi, H. Wu, A.R. Rennie, *Physical Chemistry Chemical Physics* 21 (2019) 25945–25951.
- [61] N.Y.D. Li, Š. Perutková, A. Iglič, M. Rappolt, *Elektrotehniski Vestnik/Electrotechnical Review* 84 (2017) 69–75.
- [62] S. Rabiej, M. Rabiej, *Polimery* 56 (2011) 662–670.
- [63] H. van Koningsveld, *Recueil des Travaux Chimiques des Pays-Bas* 87 (1968) 243–254.
- [64] T.J. Tyree, R. Dan, R.E. Thorne, *Acta Crystallographica Section D: Structural Biology* 74 (2018) 471–479.
- [65] O.O. Mykhaylyk, K.W. Smith, C.M. Martin, A.J. Ryan, *Journal of Applied Crystallography* 40 (2007) s297–s302.
- [66] I.A. Nyrkova, A.N. Semenov, *Soft Matter* 6 (2010) 501–516.
- [67] B. Lotz, S.Z.D. Cheng, *Polymer* 46 (2005) 577–610.
- [68] O.O. Mykhaylyk, C.M. Martin, *European Journal of Lipid Science and Technology* 111 (2009) 227–235.
- [69] A.J. Peacock, in: *Plastics Engineering, First Edition*, Marcel Dekker, New York, 2000, pp. 71–80.
- [70] M. Jasiurkowska, A. Budziak, J. Czub, M. Massalska-Arodź, S. Urban, *Liquid Crystals* 35 (2008) 513–518.
- [71] D. Sivaramakrishna, S.T. Reddy, T. Nagaraju, M.J. Swamy, *Colloids and Surfaces A: Physicochemical and Engineering Aspects* 471 (2015) 108–116.
- [72] D. Cholakova, N. Denkov, *Advances in Colloid and Interface Science* 269 (2019) 7–42.
- [73] L.A. Smith, G.B. Thomson, K.J. Roberts, D. Machin, G. McLeod, *Crystal Growth & Design* 5 (2005) 2164–2172.
- [74] P. Lo Nostro, R. Ramsch, E. Fratini, M. Lagi, F. Ridi, E. Carretti, M. Ambrosi, B.W. Ninham, P. Baglioni, *Journal of Physical Chemistry B* 111 (2007) 11714–11721.
- [75] *Physical Properties of Glycerine and Its Solutions*, Glycerine Producers' Association, New York, 1963.
- [76] C.S. Miner, N.N. Dalton, *Glycerine: An Overview*, The Soap and Detergent Association, New York, 1990.
- [77] *Chemical Properties and Derivatives of Glycerine*, Glycerine Producers' Association, New York, 1965.
- [78] L.A. Smith, A. Duncan, G.B. Thomson, K.J. Roberts, D. Machin, G. McLeod, *Journal of Crystal Growth* 263 (2004) 480–490.
- [79] H. Nakagawa, T. Oyama, *Frontiers in Chemistry* 7 (2019) 1–9.
- [80] C.C. Ruiz, L. Díaz-López, J. Aguiar, L. Díaz-López, J. Aguiar, *Journal of Dispersion Science and Technology* 29 (2008) 266–273.
- [81] Y. Hayashi, Y.E. Ryabov, A. Gutina, Y. Feldman, *AIP Conference Proceedings* 708 (2004) 671–672.
- [82] X. He, A. Fowler, M. Toner, *Journal of Applied Physics* 100 (2006) 074702.
- [83] L. Ninni, M.S. Camargo, A.J.A. Meirelles, *Journal of Chemical and Engineering Data* 45 (2000) 654–660.
- [84] O. Fysun, M. Stoeckel, K.J.F. Thienel, F. Wäschle, S. Palzer, J. Hinrichs, *Chemie Ingenieur Technik* 87 (2015) 1327–1333.
- [85] A.V. Egorov, A.P. Lyubartsev, A. Laaksonen, *Journal of Physical Chemistry B* 115 (2011) 14572–14581.
- [86] C. Marcolli, T. Peter, *Atmospheric Chemistry and Physics Discussions* 5 (2005) 1501–1527.
- [87] Y. Long, R.A. Shanks, Z.H. Stachurski, *Progress in Polymer Science* 20 (1995) 651–701.

Figure captions.

Figure 1. A) 2 wt% SDS in glycerol forming a free-standing gelled solution after heating to 60 °C and cooling quiescently to room temperature for 4 hours. B) Polarised optical microscopy image of the gelled 2 wt% SDS in glycerol. White arrows assigned by 'P' and 'A' show orientation of the polariser and the analyser plane, respectively.

Figure 2. 1D SAXD pattern of A) gelled 2 wt% SDS in glycerol mixture and B) anhydrous SDS powder with inset showing 4th order diffraction peak, where $00/G$ and $00/A$ indicate lamellar peaks of SDS-glycerol and anhydrous SDS crystal phase, respectively. The observed diffraction peaks are assigned by Miller indices corresponding to a lamellar structure.

Figure 3. A) Packing of SDS molecules in an anhydrous crystal along the layer normal. B) Schematic of electron density (ED) distribution highlighting the SDS atomic composition along the layer normal. C) Projection of the ED profile on the layer normal, indicated by vector \mathbf{n} , reproduced from corresponding structure factors calculated for crystalline anhydrous SDS [47]. D) Projection of the ED profile on the layer normal, indicated by vector \mathbf{n} , calculated from the experimental SAXD data of crystalline anhydrous SDS (Figure 2A). The set of numbers at the top of each ED profile shows $m(l)$ coefficients representing the Fourier term phase signs for all four structure factor amplitudes observed in the SAXD pattern.

Figure 4. A) The most suitable projection of electron density (ED) profile on the layer normal, indicated by vector \mathbf{n} , reconstructed from experimental SAXD lamellar peaks of SDS-glycerol crystal phase (Figure 2A), with the distance between H_1 and H_2 representing the head-to-head spacing, G indicates the region containing glycerol and D indicates the structure period (d_{001} -spacing). The set of numbers at the top of the profile shows $m(l)$ coefficients representing the Fourier term phase signs for all four structure factor amplitudes observed in the SAXD pattern. B) Schematic of the ED distribution relating the position of SDS components [head group (red) and hydrocarbon tail (grey)] and glycerol (yellow) along the SDS-glycerol layer normal. C) Packing of SDS (coloured by red and grey) and glycerol (yellow) molecules along the layer normal where glycerol lies approximately in the yellow area.

Figure 5. Background corrected WAXD patterns of centrifuged 8 wt% SDS in glycerol mixture ($\text{CuK}\alpha$ -radiation). The left inset (blue rectangle) and the right inset (red rectangle) show low-intensity lamellar peaks and characteristic fingerprint region of SDS-glycerol crystal phase.

Figure 6. Period of lamella (d_{001} -spacing) measured from SAXD patterns of n -alkyl sulfate surfactants in glycerol mixtures homologous series versus number of carbons in the surfactant hydrocarbon tail. Linear regression is extrapolated to the theoretical '0 carbon in chain' for an n -alkyl sulfate molecule exhibiting an n -alkyl sulfate-SDS crystal phase.

Figure 7. Representative polarised optical microscopy images of A) the mixed phase containing platelet, needle and ribbon crystal phases formed after heating and cooling of a 2 wt% SDS solution in a water-glycerol mixture with a water content of 2.9 wt% of the solution, B) platelet and needle crystals formed after heating and cooling of a 2 wt% SDS solution in a water-glycerol mixture with a water content of 5.6 wt% of the solution. White arrows assigned by 'P' and 'A' show orientation of the polariser and the analyser plane, respectively.

Figure 8. The dependence of relative SDS-glycerol crystal phase content (with respect to anhydrous SDS crystal phase content) on the glycerol concentration in glycerol-water solvent calculated from corresponding averages of 001_G and 001_A diffraction peak intensity observed in SAXD patterns of 2 wt% SDS in glycerol water solutions during isothermal cooling at 20 °C (Figures S12-S17). The inset contains selected representative SAXD patterns where $00/G$ and $00/A$ indicate lamellar peaks of SDS-glycerol and anhydrous SDS crystal phases: a), b) and c) correspond to representative frames obtained during isothermal cooling of mixtures containing 98.7 wt%, 97.5 wt% and 96.2 wt% glycerol in the solution, respectively.

Figure 9. Linearised Avrami kinetic plot measuring crystal growth of SDS-glycerol crystal phase from 2 wt% SDS in glycerol (red) and anhydrous SDS crystals from 2 wt% SDS in glycerol-water (93.7 wt% glycerol and 6.3 wt% water in the solution) (blue), isothermally cooled at 20 °C and measured by time-resolved SAXS of d_{001} peak intensities (Figures S12, S17). The linear regressions (solid lines) equate to an Avrami exponent of 2.0 for SDS-glycerol phase and 3.4 for anhydrous SDS.

Tables.

Table 2: Comparison of structural parameters identified in the current work and previous literature for the *n*-alkyl sulfate-glycerol crystal phase.

	SDS (C12)		C14	C16	C18
Source of information	Matthews <i>et al.</i> [15]	This work	This work	This work	This work
Lamellar period [Å]	55.6	55.1	61.0	66.2	72.1
Thickness of glycerol region including intermolecular spacing [Å]	8	7 ^{#†}	7 [†]	7 [†]	7 [†]
Molecular tilt [degrees]	N.A.	20 ^{#†}	20 [†]	20 [†]	20 [†]
Glycerol: SDS stoichiometry	1.5-2.0	≤1:1 [†]	-	-	-
Phase characterisation	Paracrystalline mesophase	Co-crystal	Co-crystal	Co-crystal	Co-crystal

[#] Estimated through determination of sublayer region within the electron density profile reconstructed from diffraction data

[†] Estimated through sublayer depth of *n*-alkyl sulfate homologues, Sublayer values and tilt represent maximum values due to limitations in determining intermolecular spacing within the sublayer.

Co-assembly and Structure of Sodium Dodecylsulfate and other *n*-Alkyl Sulfates in Glycerol: *n*-Alkyl Sulfates-Glycerol Crystal Phase

James Cosby^a, Pierre Starck^b, Dave Littlewood^b, Oleksandr O. Mykhaylyk^{a*} and Anthony J. Ryan^a

^aDepartment of Chemistry, The University of Sheffield, Sheffield, S3 7HF, U.K.

^bUnilever Research Port Sunlight, Quarry Road East, Bebington, Wirral CH63 3JW, U.K.

*Corresponding author. E-mail: O.Mykhaylyk@sheffield.ac.uk Tel: +44 (0)114 2229418

Supplementary material

Analysis of experimental SAXD patterns

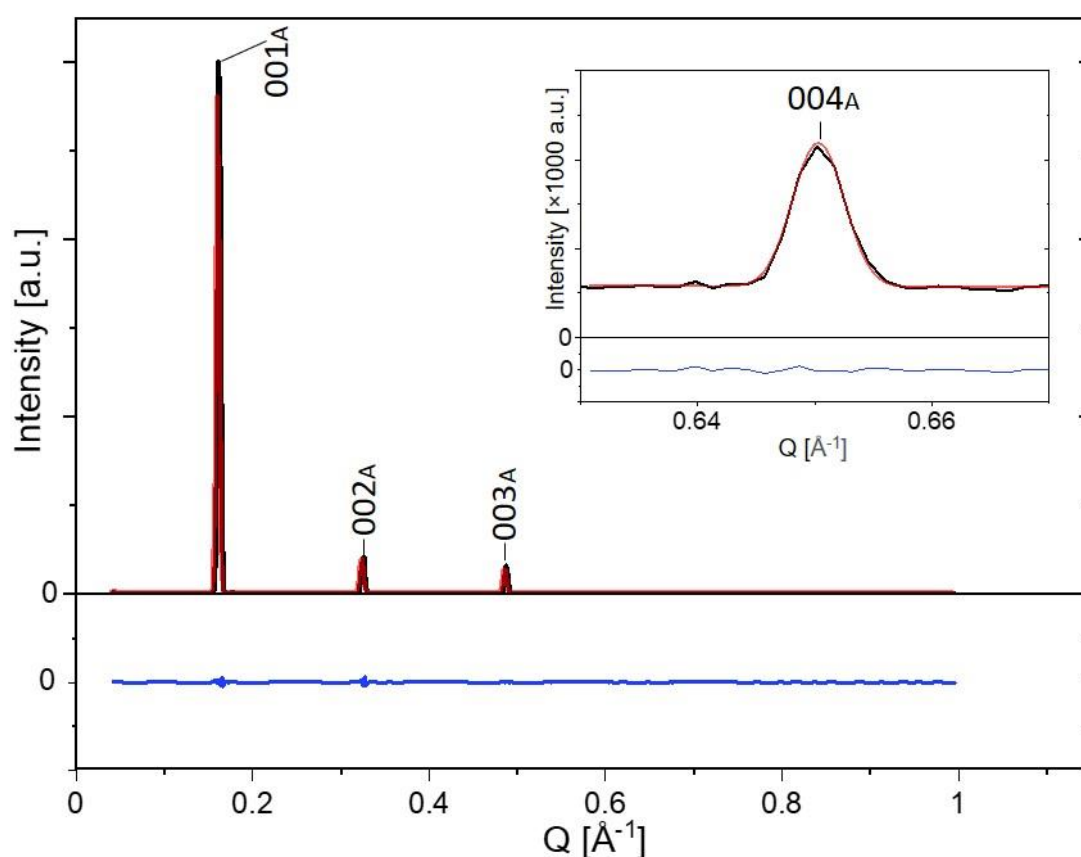


Figure S1. Peak fitting for sodium dodecylsulfate (C12) (SDS) powder data: experimental SAXD pattern (black line) with diffraction peaks and scattering background fitted by pseudo-Voigt functions and an asymmetric least square smoothing, respectively (red line). Inset shows enhanced area containing 4th order lamellar peak. The diffraction peaks are labelled by Miller indices (Table S1). The blue curve at the bottom shows residuals from the profile fitting.

Table S1. Output of the diffraction peak fitting (peak position, d -spacing and intensity) for SDS powder with crystal phase assignment and Miller indexing.

$q, \text{\AA}^{-1}$	d -spacing, \AA	Crystal phase	Miller index	Normalised intensity
0.1627	38.62	anhydrous SDS	001 _A	100
0.3256	19.30	anhydrous SDS	002 _A	6.88
0.4879	12.88	anhydrous SDS	003 _A	5.01
0.6504	9.66	anhydrous SDS	004 _A	0.03

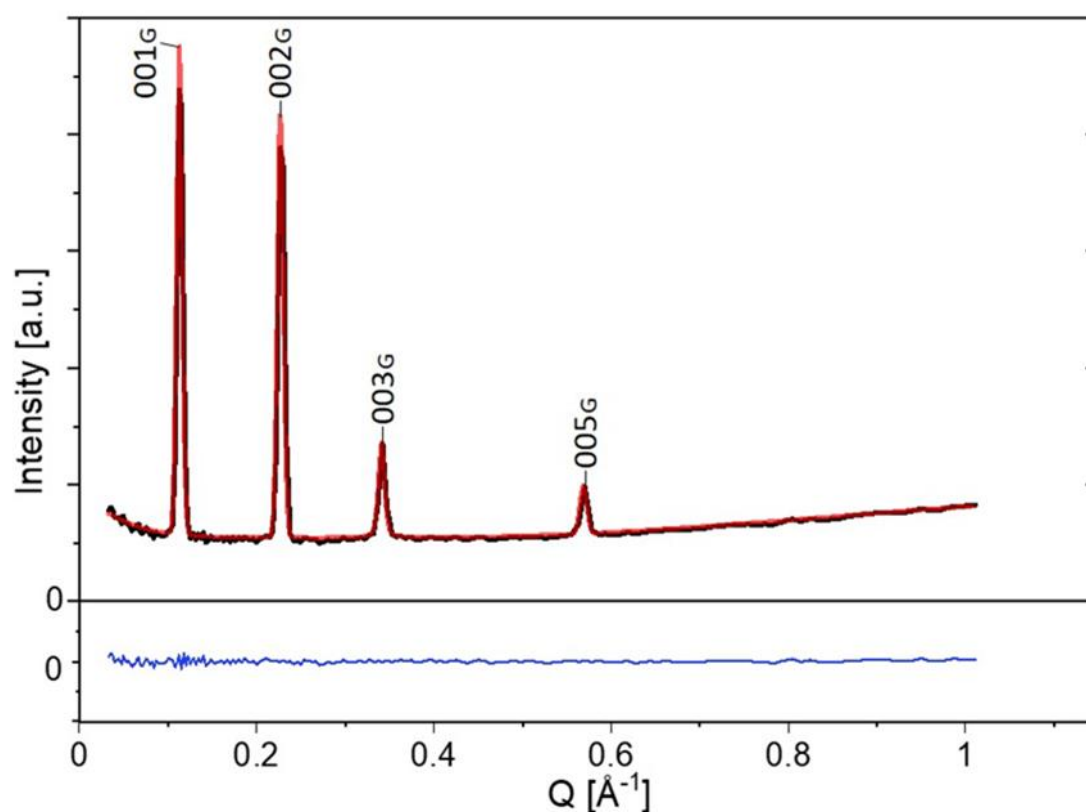


Figure S2. Peak fitting for 2 wt% SDS-glycerol gel: experimental SAXD pattern (black line) with diffraction peaks and scattering background fitted by pseudo-Voigt functions and an asymmetric least square smoothing, respectively (red line). The diffraction peaks are labelled by Miller indices (Table S2). The blue curve at the bottom shows residuals from the profile fitting.

Table S2. Output of the diffraction peak fitting (peak position, d -spacing and intensity) for 2 wt% SDS-glycerol gel with crystal phase assignment and Miller indexing.

$q, \text{\AA}^{-1}$	d -spacing, \AA	Crystal phase	Miller index	Normalised intensity
0.1140	55.14	SDS-glycerol crystal	001 _G	100
0.2280	27.56	SDS-glycerol crystal	002 _G	91.0
0.3419	18.38	SDS-glycerol crystal	003 _G	19.47
0.5699	11.03	SDS-glycerol crystal	005 _G	9.79

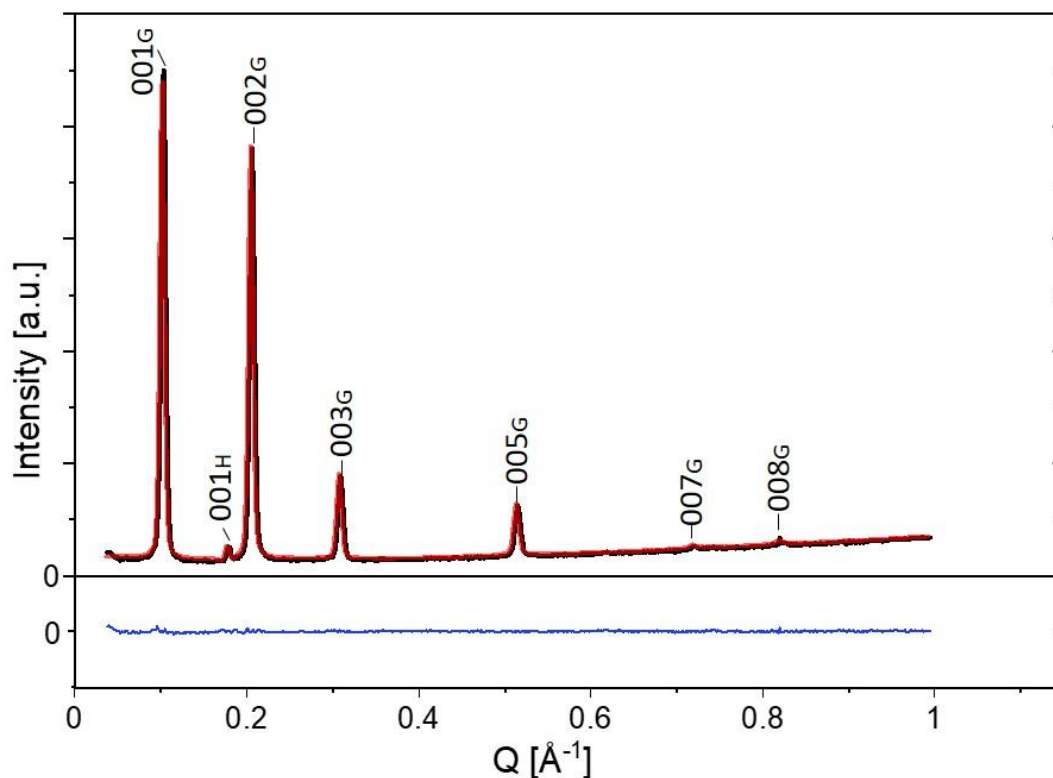


Figure S3. Peak fitting for 2 wt% sodium tetradecylsulfate (C14) (STDS)-glycerol gel: experimental SAXD pattern (black line) with diffraction peaks and scattering background fitted by pseudo-Voigt functions and an asymmetric least square smoothing, respectively (red line). The diffraction peaks are labelled by Miller indices (Table S3). The blue curve at the bottom shows residuals from the profile fitting.

Table S3. Output of the diffraction peak fitting (peak position, d -spacing and intensity) for 2 wt% STDS-glycerol gel with crystal phase assignment and Miller indexing.

$q, \text{\AA}^{-1}$	d -spacing, \AA	Crystal phase	Miller index	Normalised intensity
0.10296	61.03	STDS-glycerol crystal	001 _G	100
0.17876	35.15	STDS+H ₂ O*	001 _H	84.06
0.20618	30.47	STDS-glycerol crystal	002 _G	2.26
0.30897	20.34	STDS-glycerol crystal	003 _G	17.19
0.51507	12.20	STDS-glycerol crystal	005 _G	10.51
0.72019	8.72	STDS-glycerol crystal	007 _G	0.71
0.82136	7.65	STDS-glycerol crystal	008 _G	0.75

*Hydrous STDS with indeterminate hydration with d -spacing akin to Prins and Prins [1].

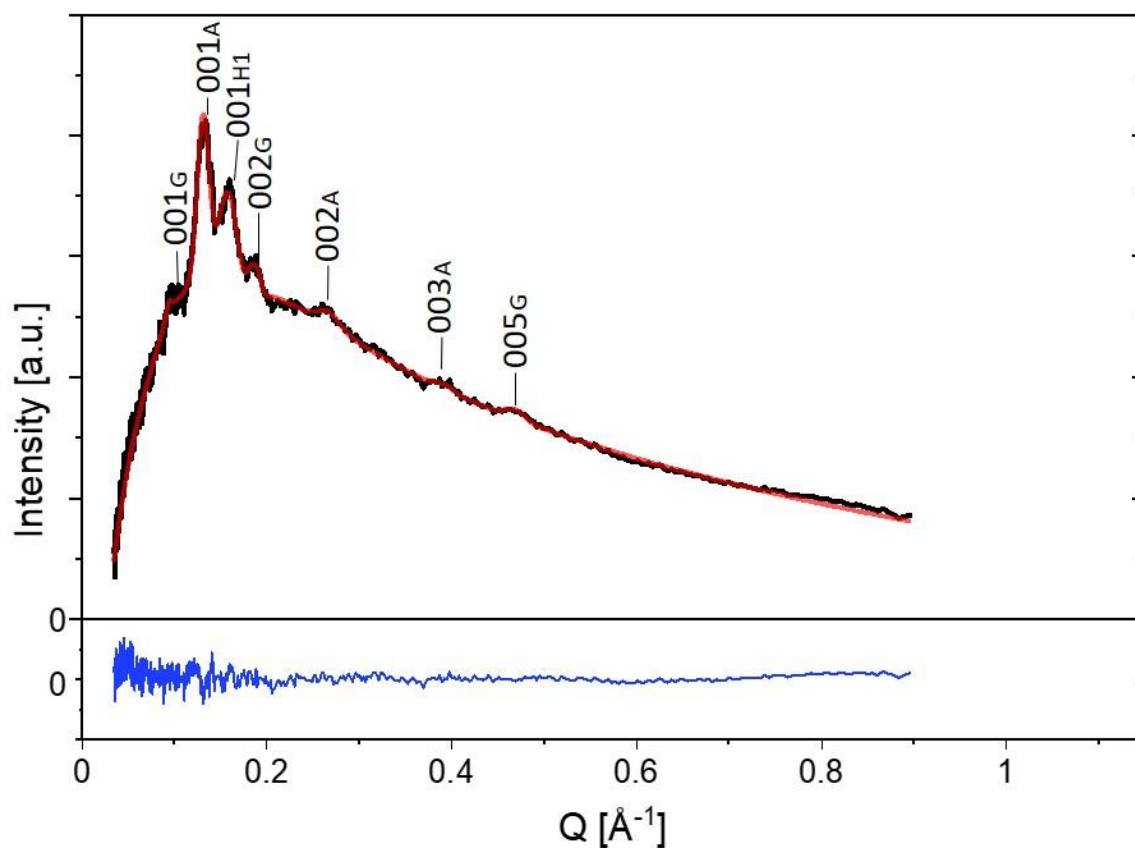


Figure S4. Peak fitting for 2 wt% sodium hexadecylsulfate (C16) (SHDS)-glycerol gel: experimental SAXD pattern (black line) with diffraction peaks and scattering background fitted by pseudo-Voigt functions and an asymmetric least square smoothing, respectively (red line). The diffraction peaks are labelled by Miller indices (Table S4). The blue curve at the bottom shows residuals of the profile fitting.

Table S4. Output of the diffraction peak fitting (peak position, d -spacing and intensity) for 2 wt% SHDS-glycerol gel with crystal phase assignment and Miller indexing.

$q, \text{\AA}^{-1}$	d -spacing, \AA	Crystal phase	Miller index	Normalised intensity
0.0949	66.21	SHDS-glycerol crystal	001G	11.6
0.1318	47.66	anhydrous SHDS	001A	100
0.1581	39.72	SHDS+1H ₂ O*	001H1	49.1
0.1869	33.61	SHDS-glycerol crystal	002G	12.3
0.2678	23.45	anhydrous SHDS	002A	10.3
0.3921	16.01	SHDS-glycerol crystal	003A	2.29
0.4699	13.37	SHDS-glycerol crystal	005G	5.28

*Hydrus SHDS with d -spacing resembling the monohydrate polymorph as described by Rawlings and Lingafelter [2].

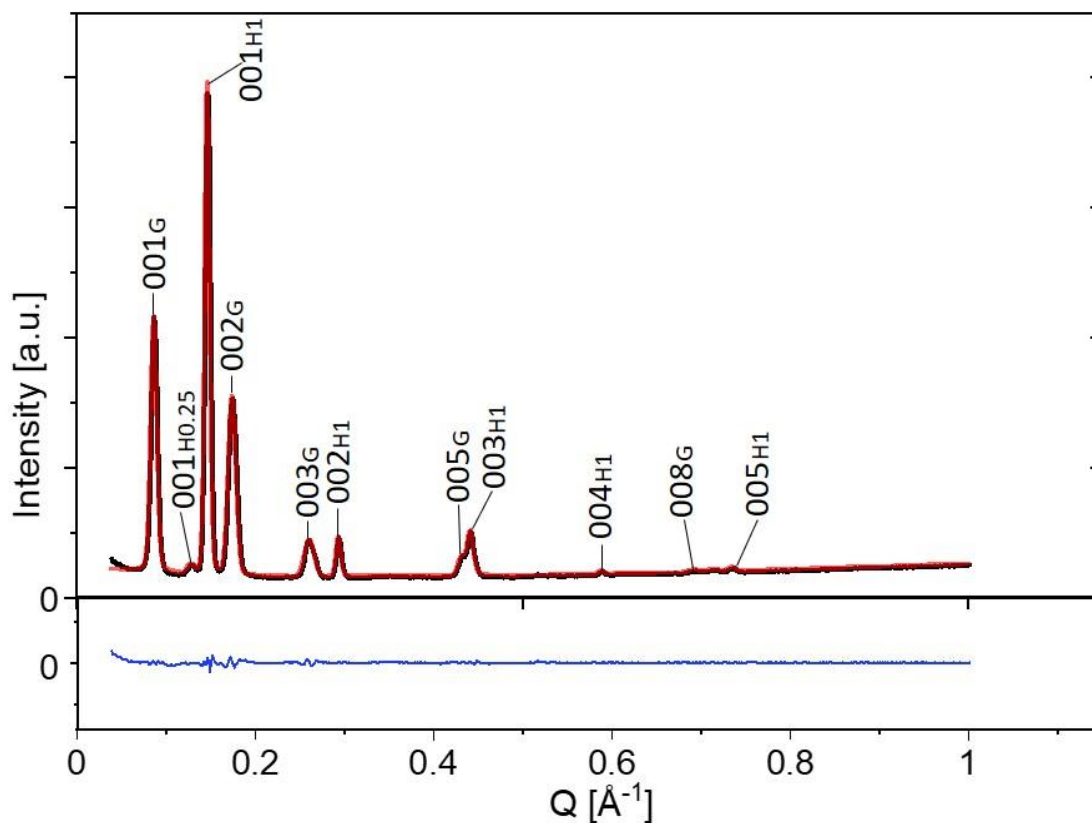


Figure S5. Peak fitting for 2 wt% sodium octadecylsulfate (C18) (SODS)-glycerol gel: experimental SAXD pattern (black line) with diffraction peaks and scattering background fitted by pseudo-Voigt functions and an asymmetric least square smoothing, respectively (red line). The diffraction peaks are labelled by Miller indices (Table S5). The blue curve at the bottom shows residuals of the profile fitting.

Table S5. Output of the diffraction peak fitting (peak position, d -spacing and intensity) data for 2 wt% SODS-glycerol gel with crystal phase assignment and Miller indexing.

q , Å ⁻¹	d -spacing, Å	Crystal phase	Miller index	Normalised intensity
0.0871	72.08	SODS-glycerol crystal	001G	51.7
0.1284	48.93	SODS+0.25H ₂ O*	001H0.25	1.33
0.1472	42.67	SODS+1H ₂ O†	001H1	100
0.1750	35.89	SODS-glycerol crystal	002G	35.9
0.2616	24.02	SODS-glycerol crystal	003G	7.37
0.2944	21.34	SODS+1H ₂ O	002H1	8.06
0.4321	14.54	SODS-glycerol crystal	005G	3.38
0.4421	14.21	SODS+1H ₂ O	003H1	9.16
0.5894	10.66	SODS+1H ₂ O	004H1	0.54
0.6932	9.06	SODS-glycerol crystal	008G	0.47
0.7361	8.54	SODS+1H ₂ O	005H1	0.85

*Hydrous SODS with d -spacing resembling the quarterhydrate polymorph as described by Rawlings and Lingafelter [2].

†Hydrous SODS with d -spacing resembling the monohydrate polymorph as described by Rawlings and Lingafelter [2].

Projection of electron density profile on the layer normal

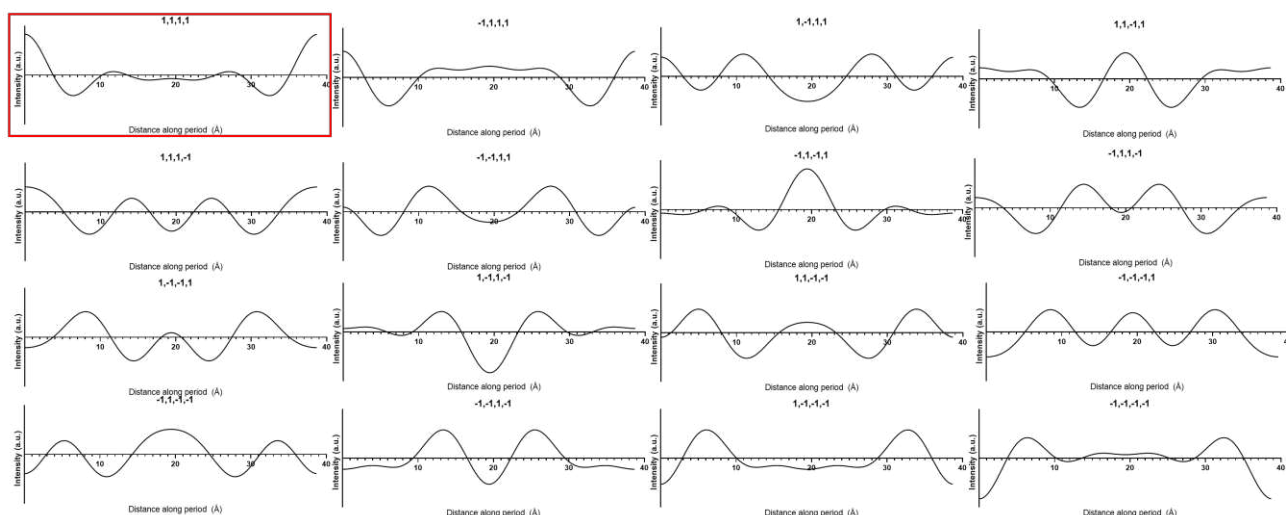


Figure S6. Electron density profiles calculated for different sets of phase signs $m(l)$ (see eq 4 in the main text) using crystal structure of anhydrous SDS reported in literature [3]. $m(l)$ signs are shown at the top of each profile. For example, a set of signs 1, 1, -1, 1 of the top right profile indicates that $m(1) = 1$ (that is '+'), $m(2) = 1$, $m(3) = -1$ (that is '-') and $m(4) = 1$. A profile framed by the red rectangle corresponds to the electron density of the anhydrous SDS crystal along the layer normal.

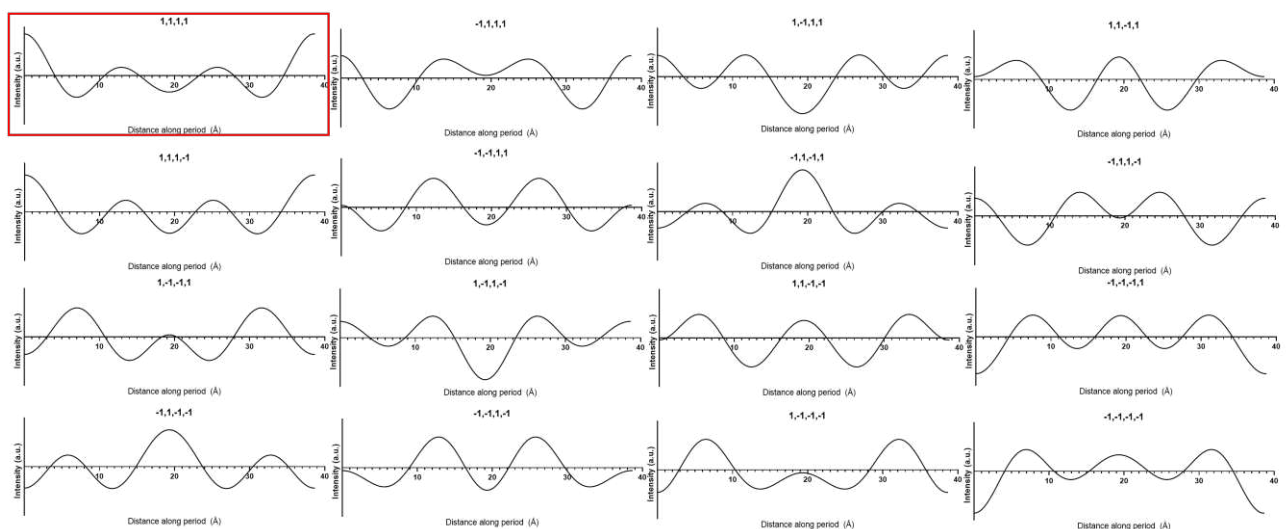


Figure S7. Electron density profiles calculated for different sets of phase signs $m(l)$ (see eq 4 in the main text) using structure factor amplitudes measured from SAXD pattern recorded for SDS powder (Figures 2B and S1). $m(l)$ signs are shown at the top of each profile. A profile framed by the red rectangle corresponds to the electron density of the anhydrous SDS crystal along the layer normal.

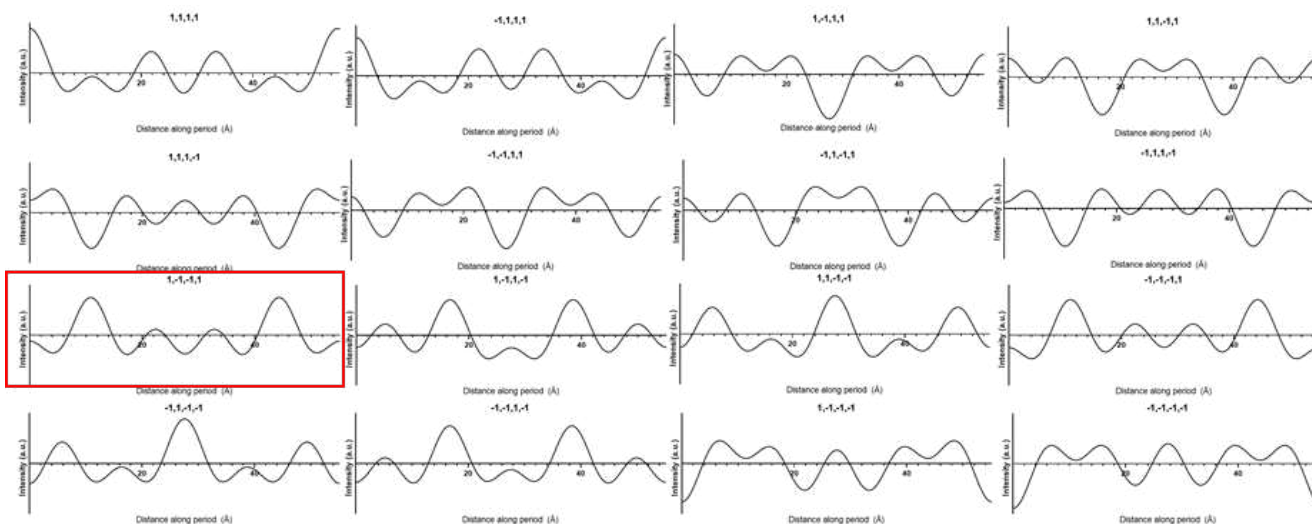


Figure S8. Electron density profiles calculated for different sets of phase signs $m(l)$ (see eq 4 in the main text) using structure factor amplitudes measured from SAXD pattern of SDS-glycerol crystal phase (Figures 2A and S2). $m(l)$ signs are shown at the top of each profile. For example, a set of signs 1, 1, -1, 1 of the top right profile indicates that $m(1) = 1$, $m(2) = 1$, $m(3) = -1$ and $m(5) = 1$, where $m(4)$ is omitted because of low or 'zero' intensity of the 004_g diffraction peak (Figures 2A and S2). The red rectangle indicates profile of electron density along the layer normal chosen for the crystal structure.

1D WAXS scattering patterns

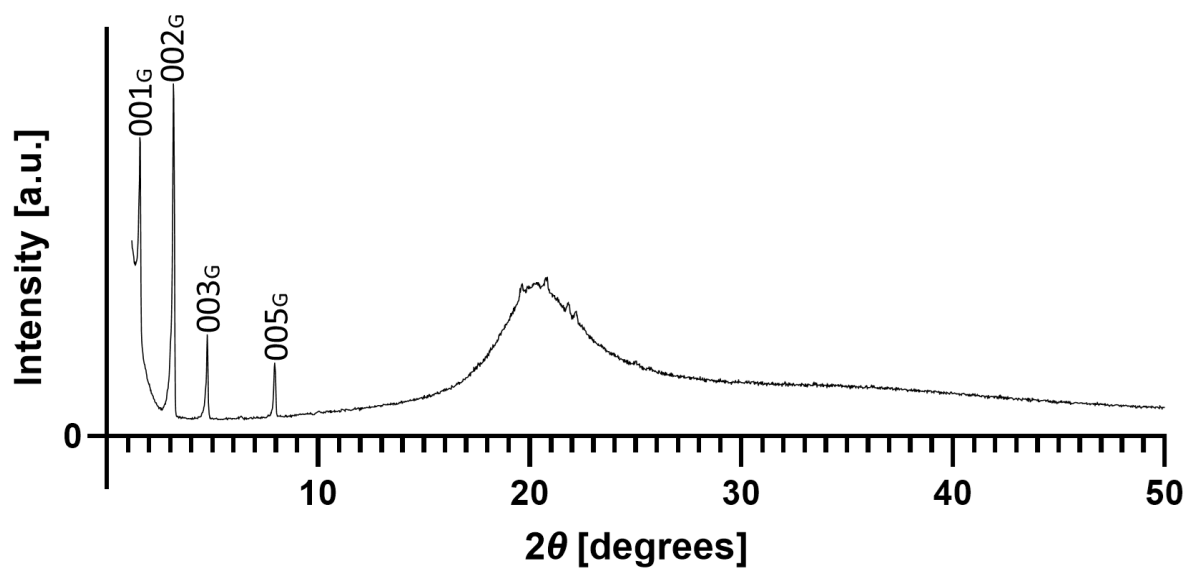


Figure S9. Scattering pattern of 8 wt% SDS-glycerol gel after centrifugation recorded by X-ray diffractometer ($\text{CuK}\alpha$ -radiation) using Bragg-Brentano geometry. Miller indices are assigned to lamellar diffraction peaks corresponding to SDS-glycerol crystal phase.

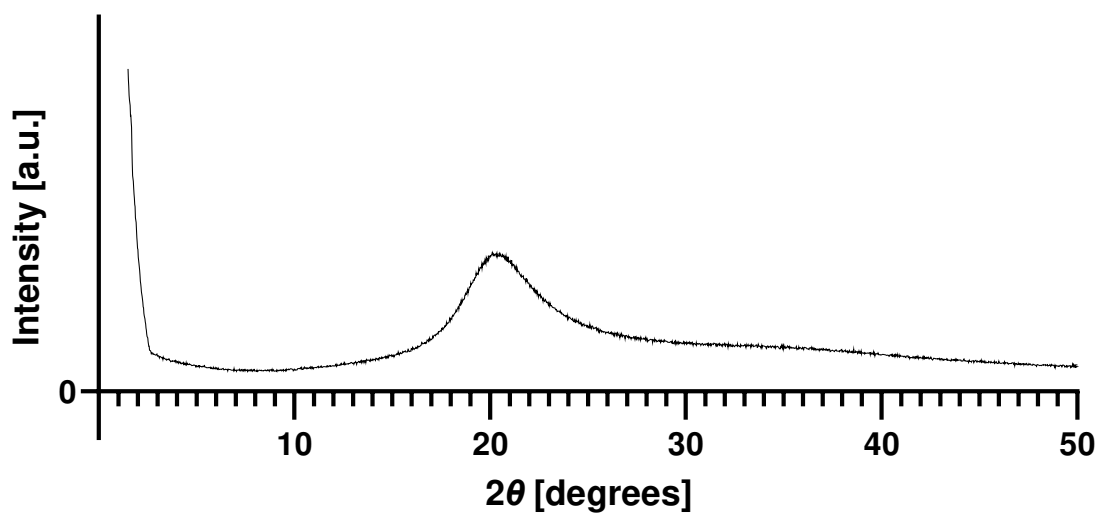


Figure S10. Scattering pattern of liquid glycerol recorded by X-ray diffractometer ($\text{CuK}\alpha$ -radiation) using Bragg-Brentano geometry.

Microscopy images of gelled *n*-alkyl sulfate solutions in glycerol

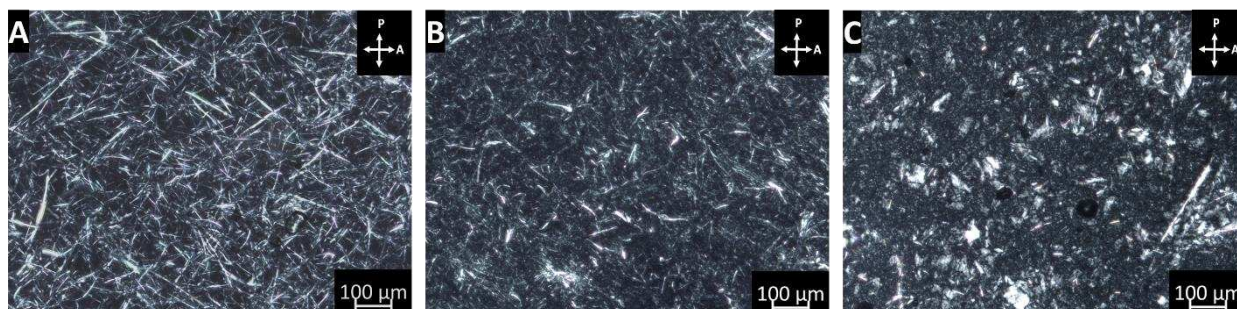


Figure S11. Polarised optical microscopy image of the gelled 4 wt% A) SDS (C12)-glycerol mixture comprised of ribbons of the SDS-glycerol crystal phase, B) STDS (C14)-glycerol mixture comprised of mixed phases of ribbons, needles, and platelets, C) SODS (C18)-glycerol mixture comprised of ribbons, needles, and platelets. The ribbon phase corresponds to *n*-alkyl sulfate-glycerol crystal phase, whereas platelets and needles correspond to anhydrous and hydrated crystals of varying stoichiometry, respectively. White arrows assigned by 'P' and 'A' show orientation of the polariser and the analyser plane, respectively.

Time-resolved 1D SAXS patterns during isothermal cooling with peak fit analysis

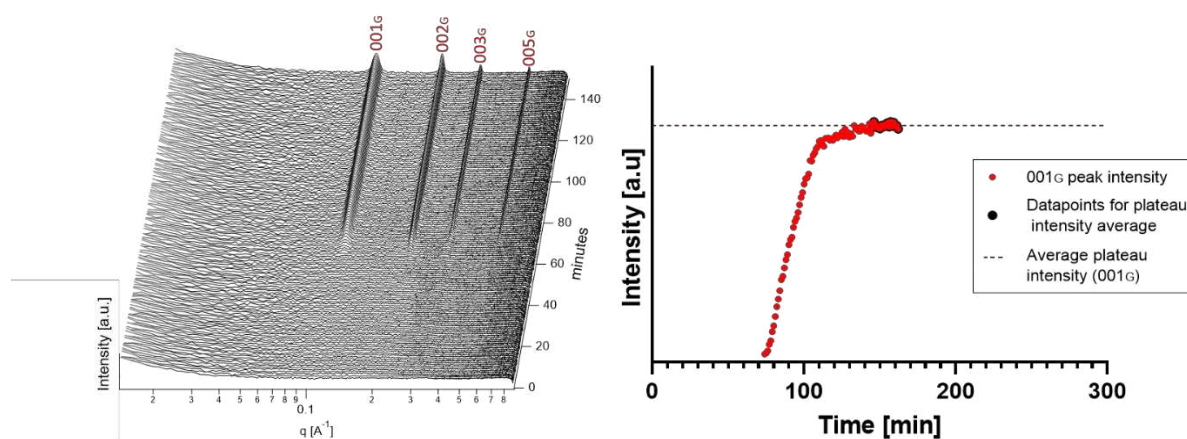


Figure S12. Time-resolved 1D SAXS pattern of 2 wt% SDS in glycerol during isothermal cooling at 20 °C (left) and 001_G peak intensity versus the cooling time (right). Miller indices are assigned to lamellar diffraction peaks of the SDS-glycerol crystal phase.

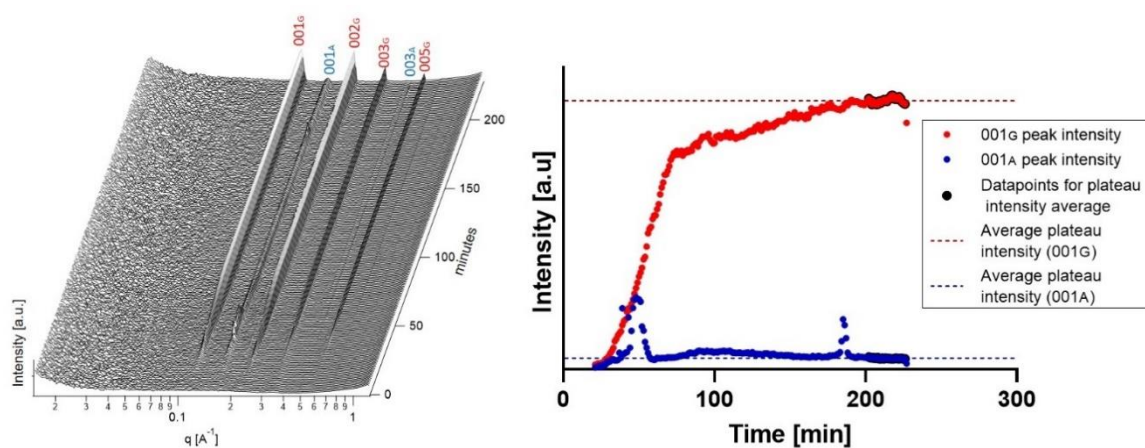


Figure S13. Time-resolved 1D SAXS pattern of 2 wt% SDS in glycerol-water solvent (98.7 wt% glycerol and 1.3 wt% water in the solution) during isothermal cooling at 20 °C (left), and 001_G and 001_A peak intensity versus the cooling time (right). Miller indices are assigned to lamellar diffraction peaks of the SDS-glycerol crystal phase, 001_G, and the anhydrous SDS crystals, 001_A.

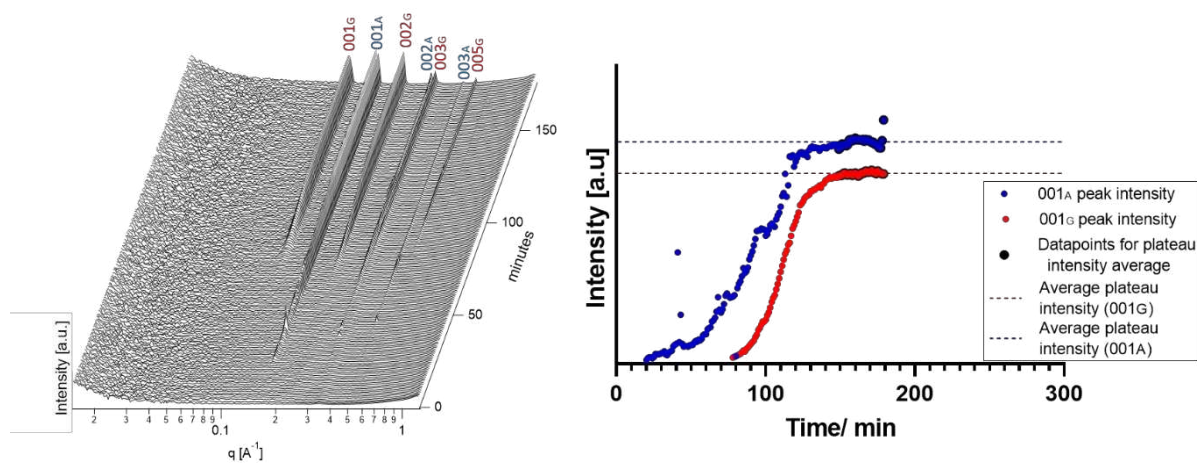


Figure S14. Time-resolved 1D SAXS pattern of 2 wt% SDS in glycerol-water solvent (97.5 wt% glycerol and 2.5 wt% water in the solution) during isothermal cooling at 20 °C (left), and 001G and 001A peak intensity versus the cooling time (right). Miller indices are assigned to lamellar diffraction peaks of the SDS-glycerol crystal phase, 00_G, and the anhydrous SDS crystals, 00_A.

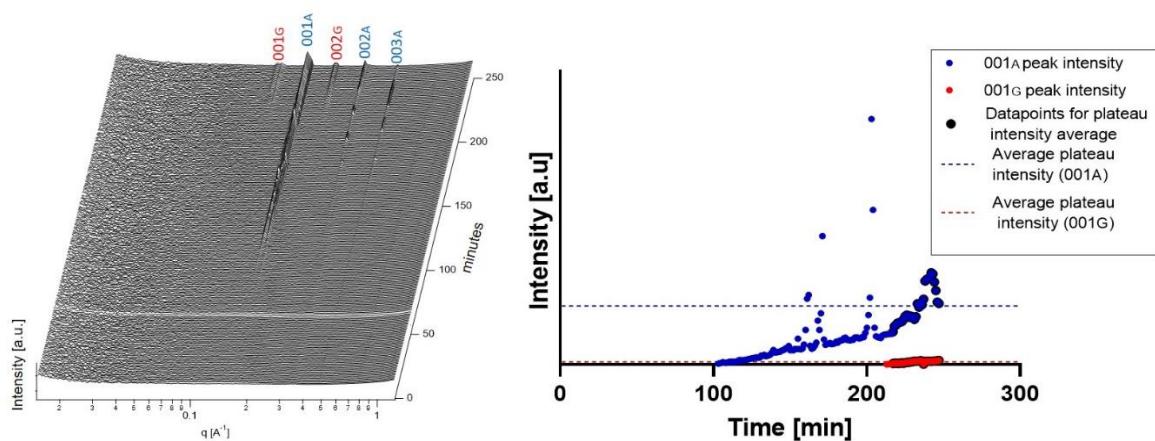


Figure S15. Time-resolved 1D SAXS pattern of 2 wt% SDS in glycerol-water solvent (96.2 wt% glycerol and 3.8 wt% water in the solution) during isothermal cooling at 20 °C (left), and 001G and 001A peak intensity versus the cooling time (right). Miller indices are assigned to lamellar diffraction peaks of the SDS-glycerol crystal phase, 00_G, and the anhydrous SDS crystals, 00_A.

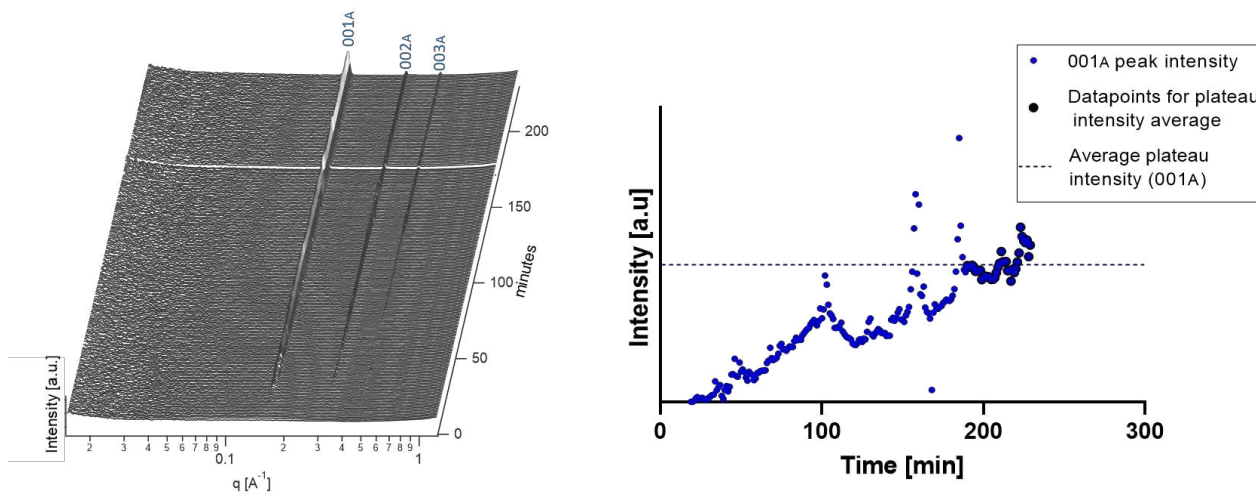


Figure S16. Time-resolved 1D SAXS pattern of 2 wt% SDS in glycerol-water solvent (95.0 wt% glycerol and 5.0 wt% water in the solution) during isothermal cooling at 20 °C (left) and 001A peak intensity versus the cooling time. Miller indices are assigned to lamellar diffraction peaks of the anhydrous SDS crystals.

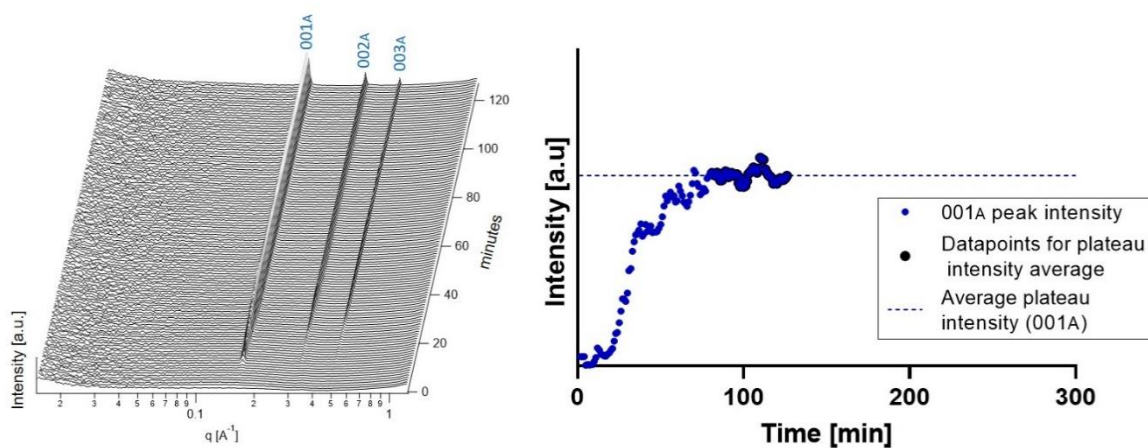


Figure S17. Time-resolved 1D SAXS pattern of 2 wt% SDS in glycerol-water solvent (93.7 wt% glycerol and 6.3 wt% water in the solution) during isothermal cooling at 20 °C (left) and 001A peak intensity versus the cooling time (right). Miller indices are assigned to lamellar diffraction peaks of the anhydrous SDS crystals.

2D SAXS pattern

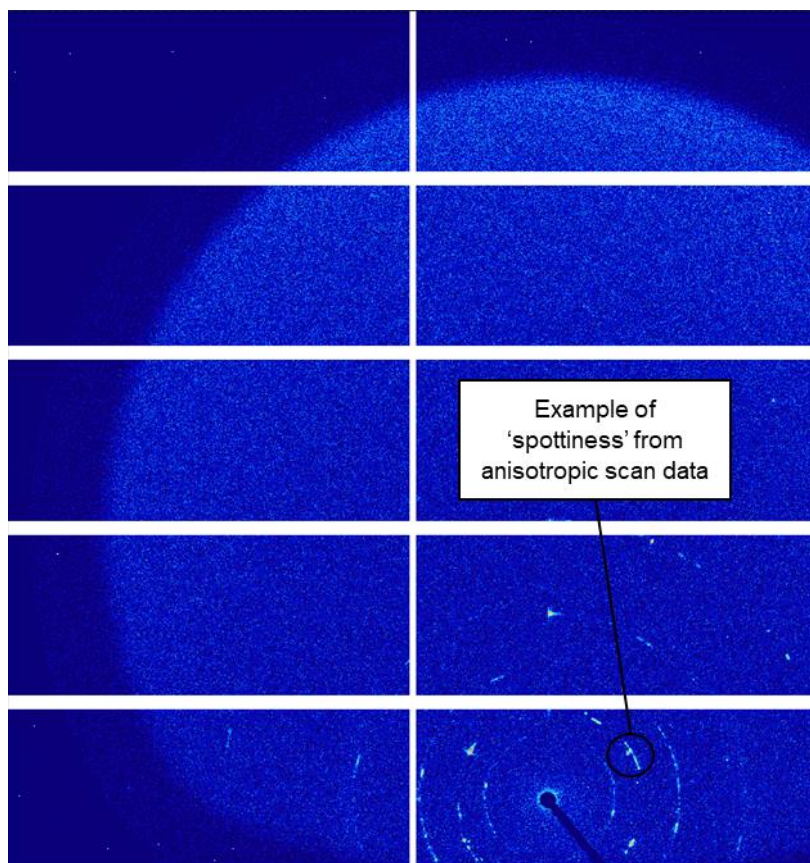


Figure S18. 2D scattering pattern of 2 wt% SDS in glycerol-water solution containing 96 wt% glycerol in the solution recorded after 246 minutes of isothermal cooling at 20 °C. The pattern shows diffraction rings with spot reflections and intensity anisotropy due to large crystal size and texture, respectively.

References

- [1] J.A. Prins, W. Prins, *Nature* 177 (1956) 535–536.
- [2] F.F. Rawlings, E.C. Lingafelter, *Journal of the American Chemical Society* 77 (1955) 870–872.
- [3] L.A. Smith, R.B. Hammond, K.J. Roberts, D. Machin, G. McLeod, *Journal of Molecular Structure* 554 (2000) 173–182.